École Doctorale des Sciences de l'Environnement d'Île-de-France

Année Universitaire 2020-2021

Modélisation Numérique de l'Écoulement Atmosphérique et Assimilation de Données

Olivier Talagrand

Cours 2

2 Avril 2021

- Additional material on numerical modelling of the atmospheric circulation. Temporal discretization.

- Numerical Weather Prediction. Present performance (mostly ECMWF)

- The meteorological observation system

- Assimilation. Basics of statistical estimation.

Physical laws governing the flow

- Conservation of mass

  $D\rho/Dt + \rho \, \mathrm{div}\underline{U} = 0$

- Conservation of energy

  $De/Dt - (p/\rho^2) \, D\rho/Dt = Q$

- Conservation of momentum

  $D\underline{U}/Dt + (1/\rho) \, \mathrm{grad}p - \underline{g} + 2 \, \underline{\Omega} \wedge \underline{U} = \underline{F}$

- Equation of state

  $f(p, \rho, e) = 0$ $\qquad\qquad$ $(p/\rho = rT, e = C_v T)$

- Conservation of mass of secondary components (water in the atmosphere, salt in the ocean, chemical species, …)

  $Dq/Dt + q \, \mathrm{div}\underline{U} = S$

These physical laws must be expressed in practice in discretized (and necessarily imperfect) form, both in space and time

A number of simplifications, in particular the hydrostatic approximation, lead to the so-called *primitive equations*, on which large-scale numerical weather prediction, and climatic simulation, are built.

More costly nonhydrostatic models are used for small scale meteorology, and are being developed for global modeling.

Integrate equation

$$dx / dt = F(x)$$

(x state vector of the model).

Timestep Δt.

Computed solution at time $n\Delta t$ denoted x_n

Forward (Euler) scheme

$$(x_{n+1} - x_n)/\Delta t = F(x_n)$$

$$x_{n+1} = x_n + \Delta t\, F(x_n)$$

Implemented on equation

$$dx / dt = i\alpha x \quad , \quad \alpha \text{ real} \qquad (1)$$

Exact solution $x(t) = x(0) \exp(i\alpha t)$

Modulus $|x(t)|$ conserved in time

Discretized solution according to forward scheme

$$x_{n+1} = (1 + i\alpha\Delta t)\, x_n$$

Modulus $|x_{n+1}| = \sqrt{(1 + \alpha^2\Delta t^2)}\, |x_n|$

increases exponentially with time.

Forward scheme is *unconditionally unstable* for Eq. (1)

Leapfrog scheme

$$(x_{n+1} - x_{n-1})/2\Delta t = F(x_n)$$
$$x_{n+1} = x_{n-1} + 2\Delta t\, F(x_n)$$

Stable for equation (1) above (*i.e.* modulus remains constant in time) provided

$$\alpha\Delta t < 1$$

Courant-Friedrichs-Lewy (CFL) condition

In a multidimensional system, the largest α will be the highest frequency that is present in the system. In a discretized system of travelling waves, the highest frequency will correspond to the fastest wave that the discretization can explicitly resolve. It will proportional to $c/\Delta x$, where c is the phase velocity of the fastest waves in the system, and Δx the mesh-size of the discretization

$$\alpha = (1/\beta)\, c/\Delta x$$

where β is an $O(1)$ numerical coefficient depending on the particular discretization scheme under consideration.

CFL condition then becomes

$$\Delta t / \Delta x < \beta / c$$

Significance : numerical propagation of signal must be at least as fast as physical propagation.

CFL condition generally applies to explicit schemes of temporal discretization

In hydrostatic atmosphere, fastest propagating wave : gravity wave with largest scale height, $c = \sqrt{(rT)} \approx 300$ $m.s^{-1}$.

$$\Delta x = 30 \text{ km} \quad \Rightarrow \Delta t = 100 \text{ s}$$

The use of *semi-implicit* schemes allows to get rid of the CFL condition, and to use longer timesteps.

Centre Européen pour les Prévisions Météorologiques à Moyen Terme (CEPMMT, Reading, GB)

(European Centre for Medium-range Weather Forecasts, ECMWF)

Depuis mars 2016 :

Troncature triangulaire TCO1279 / O1280 (résolution horizontale ≈ 9 kilomètres)

137 niveaux dans la direction verticale (0 - 80 km)

Discrétisation en éléments finis dans la direction verticale (coordonnée hybride)

Dimension du vecteur d'état correspondant > 10^9

Pas de discrétisation temporelle (schéma semi-Lagrangien semi-implicite): 450 secondes

Intégré 2 fois par jour (00 et 12 UTC) à une échéance de 10 jours

Base time: Sat 20 Mar 2021 00 UTC, Valid time: Thu 25 Mar 2021 00 UTC, - T+120 h, Area : Europe

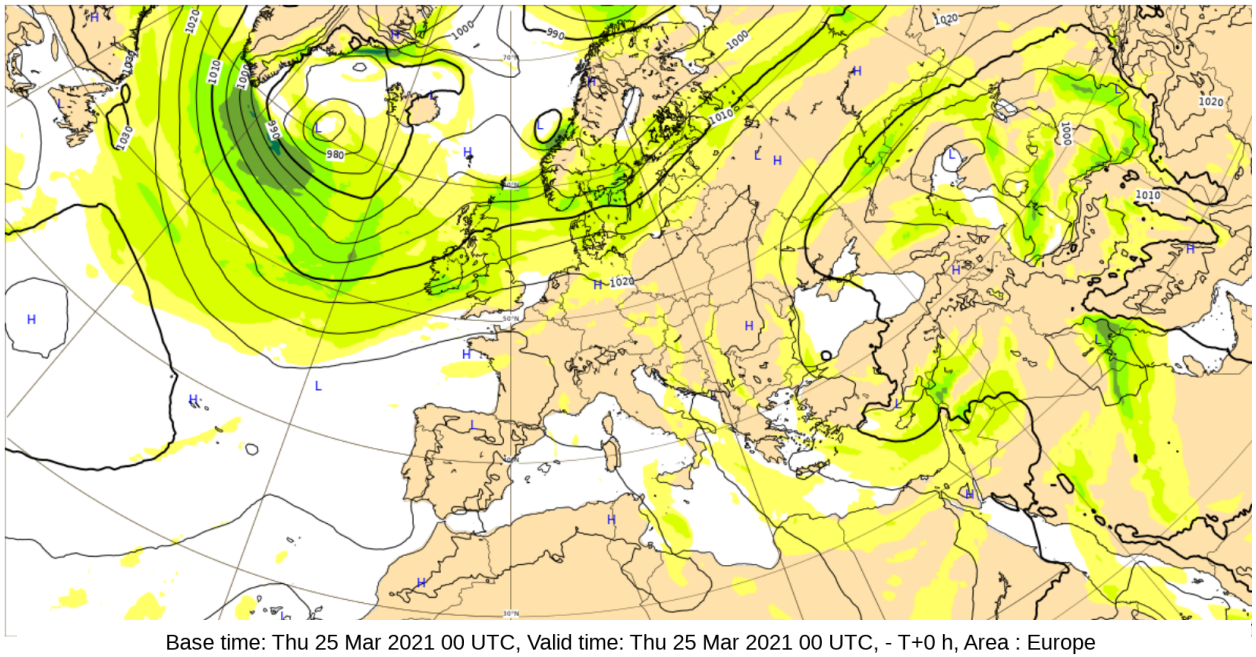

Base time: Thu 25 Mar 2021 00 UTC, Valid time: Thu 25 Mar 2021 00 UTC, - T+0 h, Area : Europe

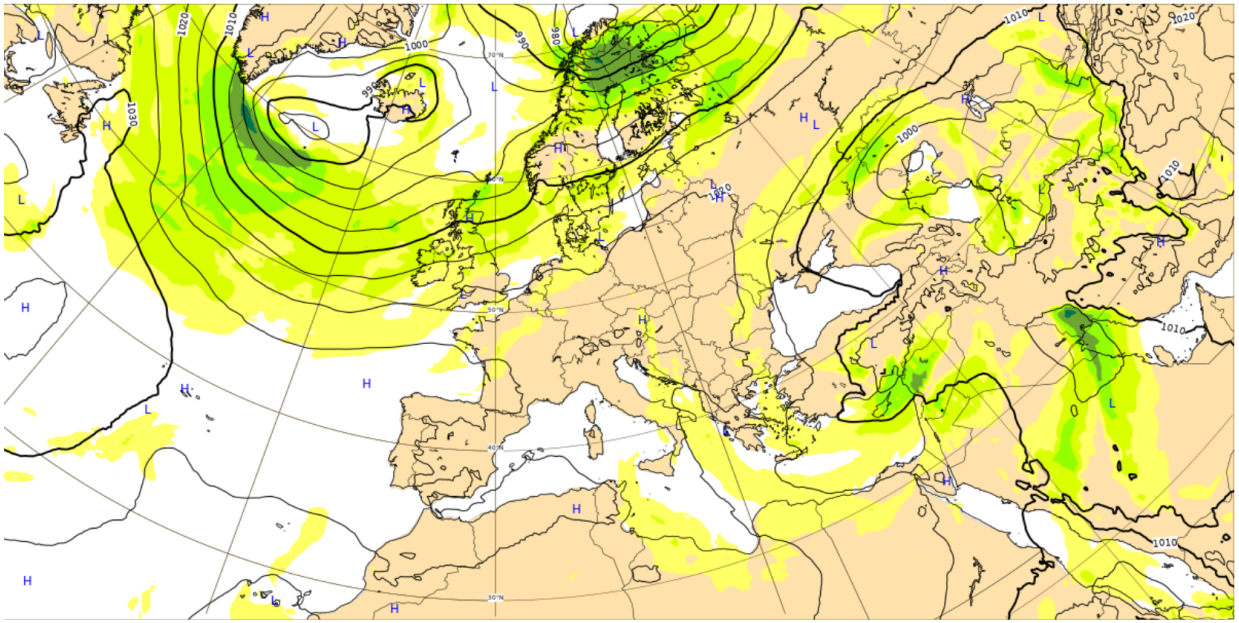

850 hPa wind speed (ms**-1)

10 15 20 25 30 40 50 60 80 100 (m/s)

Mean sea level pressure (hPa)

2021

Base time: Sat 20 Mar 2021 00 UTC, Valid time: Sat 20 Mar 2021 00 UTC, - T+0 h, Area : Europe

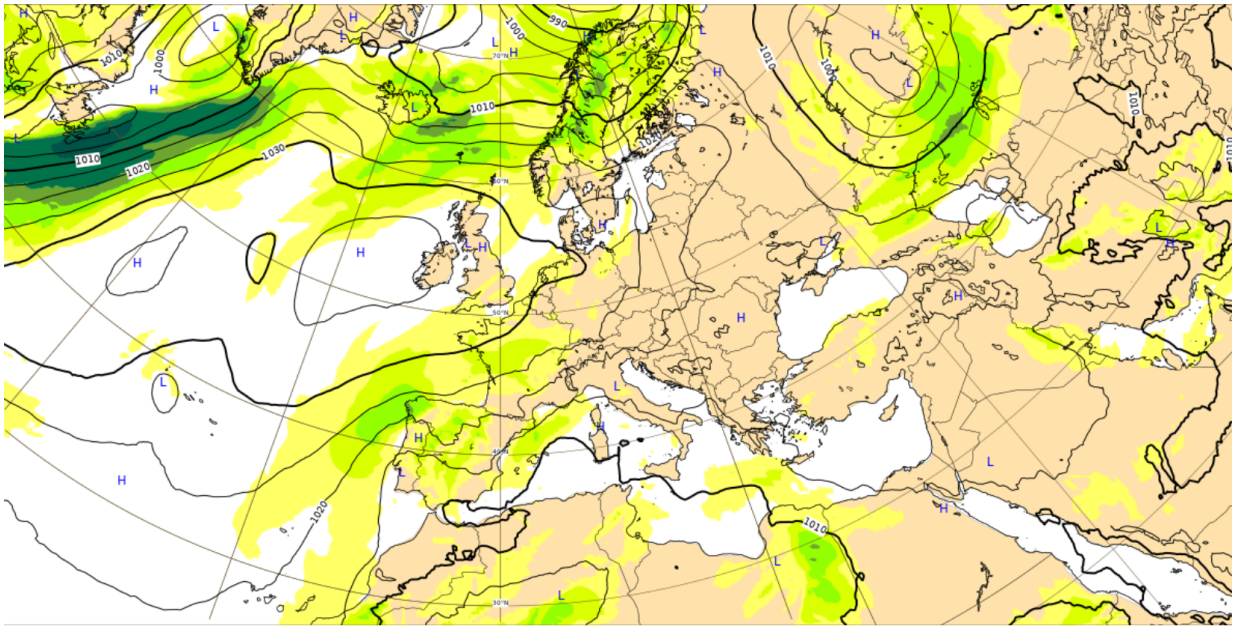

Base time: Thu 25 Mar 2021 00 UTC, Valid time: Thu 25 Mar 2021 00 UTC, - T+0 h, Area : Europe

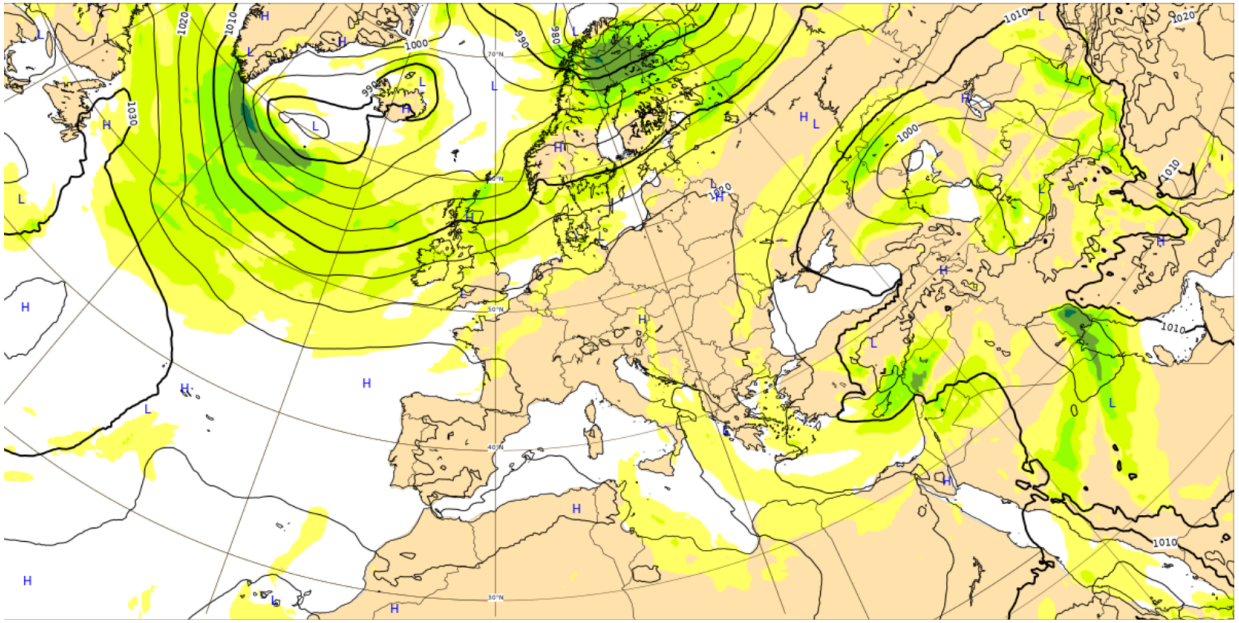

850 hPa wind speed (ms**-1)

10 15 20 25 30 40 50 60 80 100 (m/s)

Mean sea level pressure (hPa)

2021

Geopotential 500 hPa and temperature at 850 hPa

Base time: Fri 02 Apr 2021 00 UTC, Valid time: Wed 07 Apr 2021 00 UTC, - T+120 h, Area : Europe

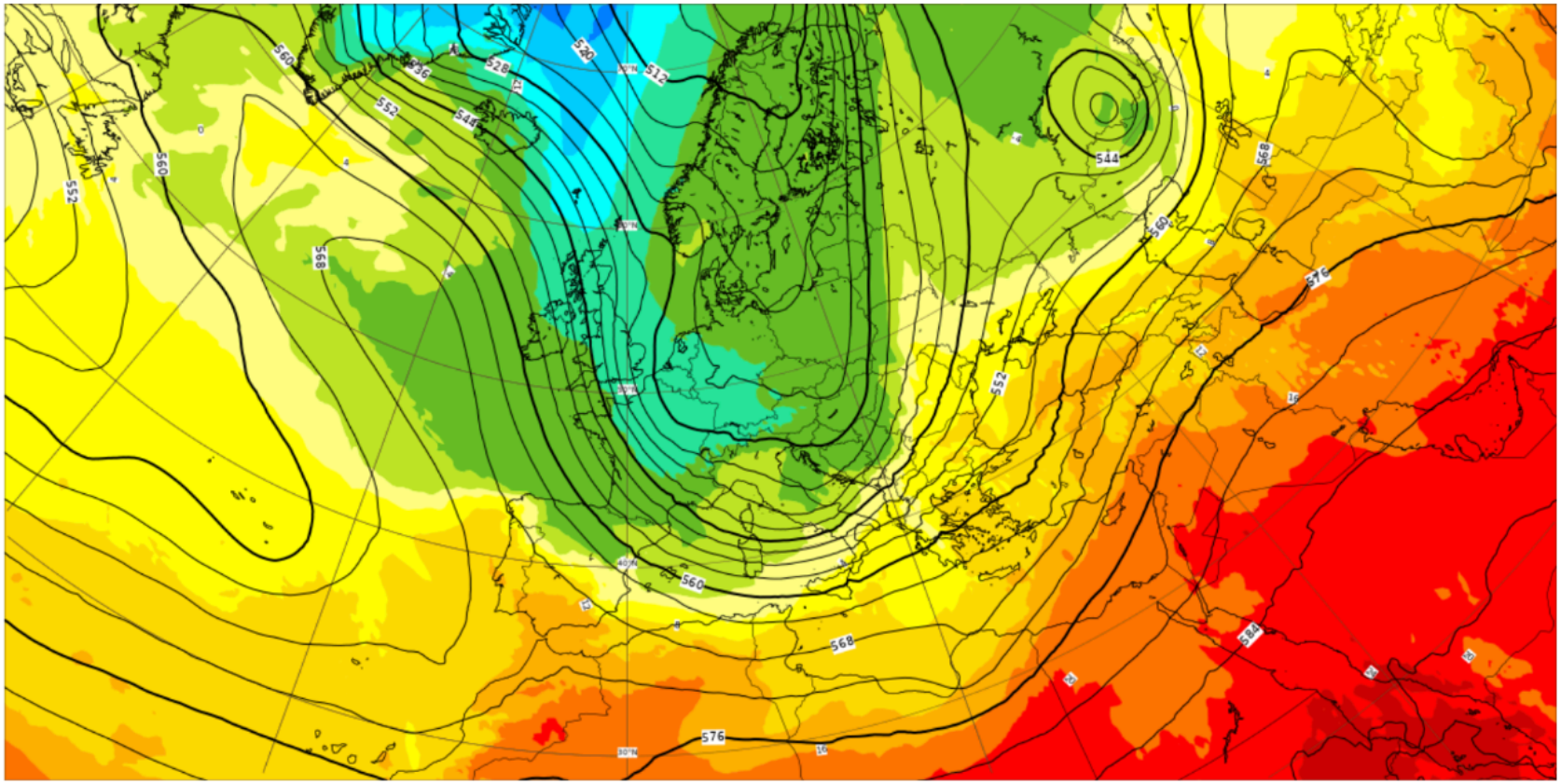

850 hPa temperature (C)

-80 -70 -60 -52 -48 -44 -40 -36 -32 -28 -24 -20 -16 -12 -8 -4 0 4 8 12 16 20 24 28 32 36 40 44 48 52 52

500 hPa geopotential (dm)

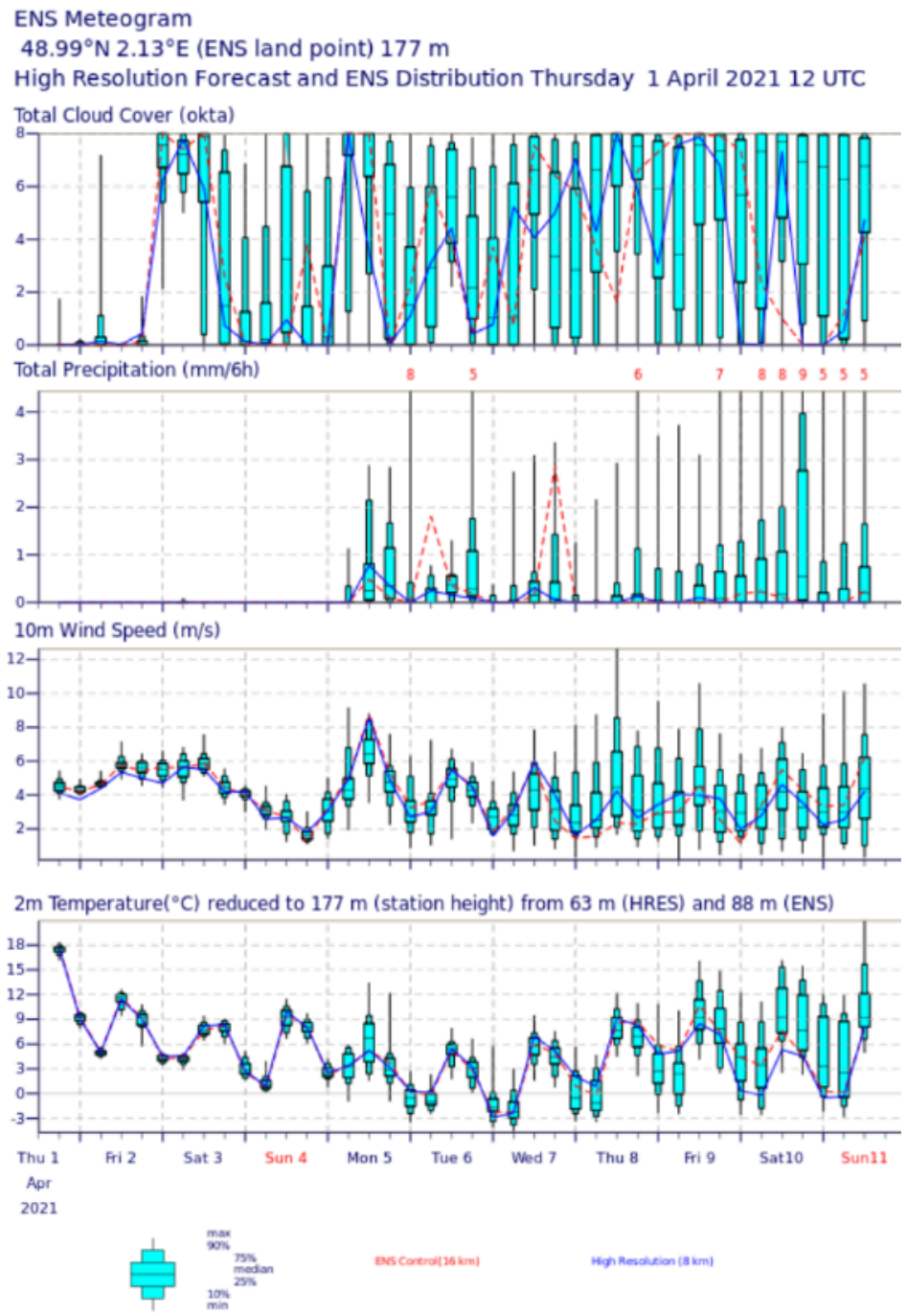
ENS Meteogram
48.99°N 2.13°E (ENS land point) 177 m
High Resolution Forecast and ENS Distribution Thursday 1 April 2021 12 UTC
Total Cloud Cover (okta)
Total Precipitation (mm/6h)
8 5 6 7 8 8 9 5 5 5
10m Wind Speed (m/s)
2m Temperature(°C) reduced to 177 m (station height) from 63 m (HRES) and 88 m (ENS)
Thu 1 Apr 2021
Fri 2
Sat 3
Sun 4
Mon 5
Tue 6
Wed 7
Thu 8
Fri 9
Sat10
Sun11
max
90%
75%
median
25%
10%
min
ENS Control(16 km)
High Resolution (8 km)

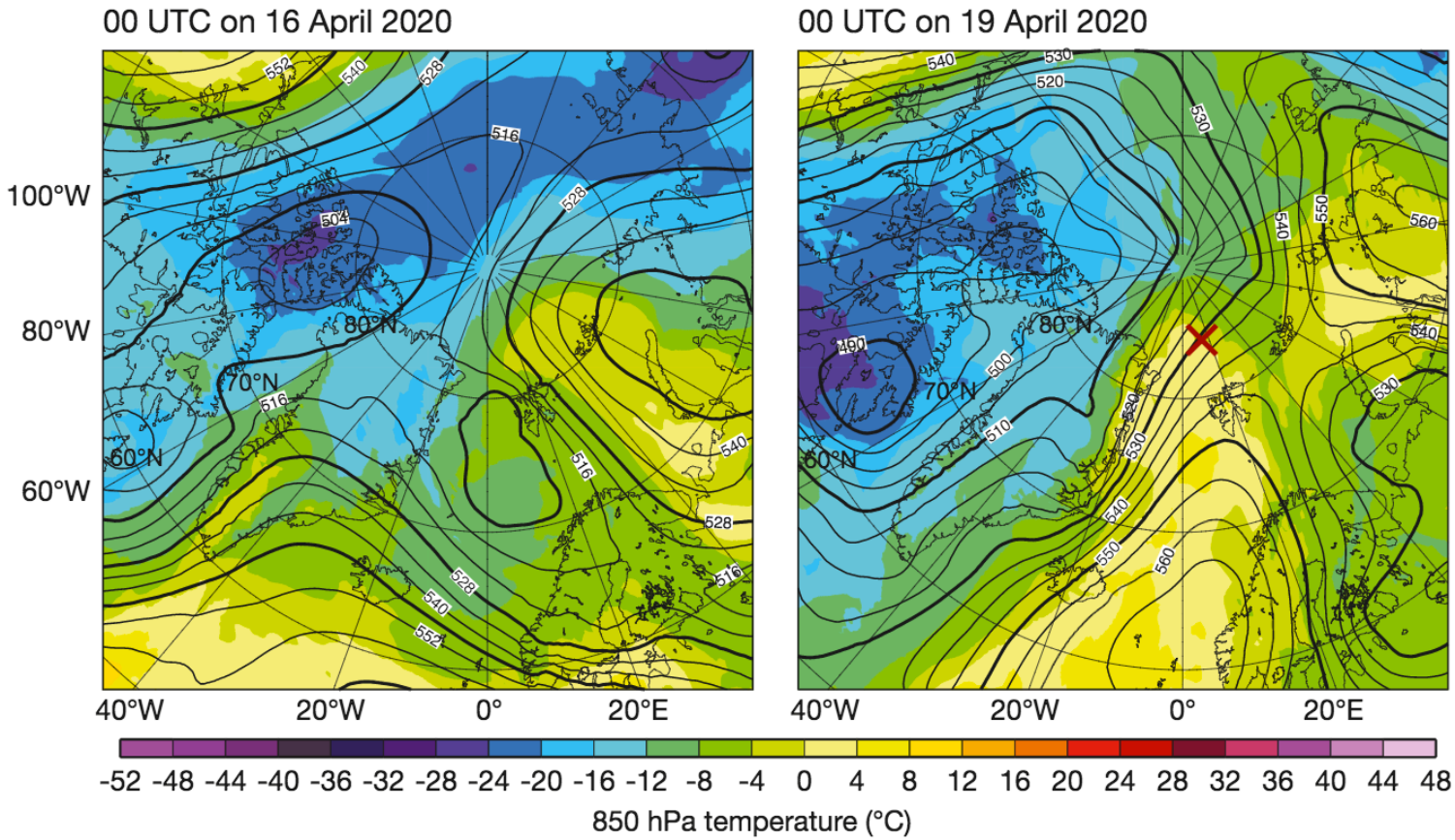

Synoptic situation on 16 and 19 April. Analysis of geopotential height at 500 hPa (contours) and temperature at 850 hPa (shading) for 00 UTC on 16 April 2020 (left) and 00 UTC on 19 April (right). The cross shows the approximate location of Polarstern on 19 April.

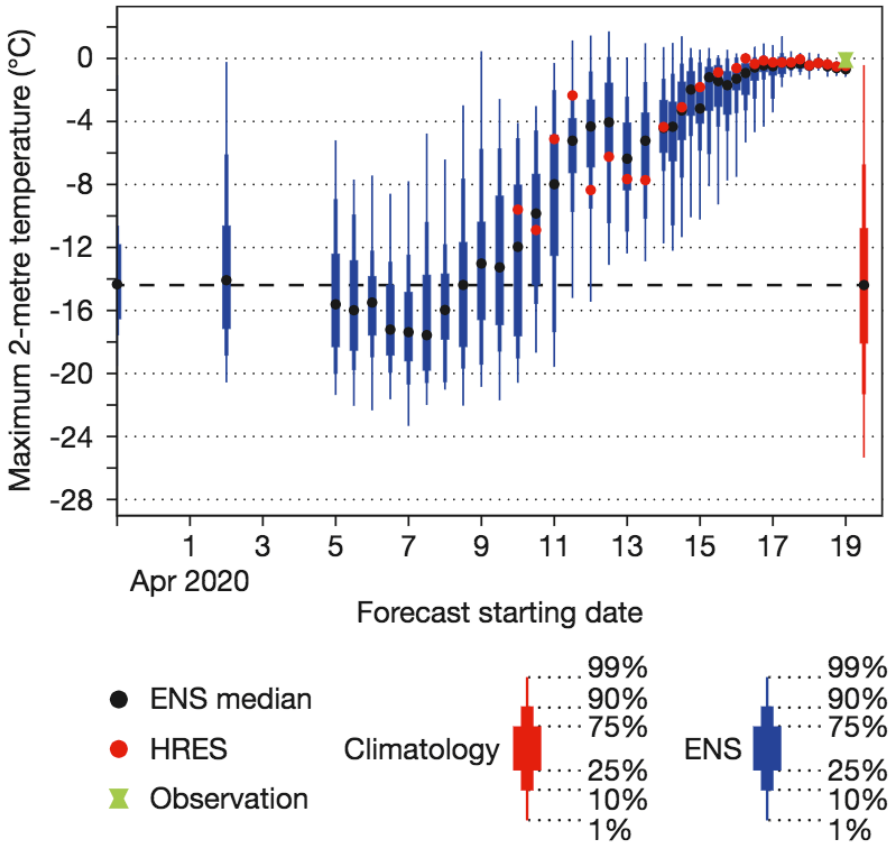

Evolution of forecasts for the 19 April warm air intrusion. The plot shows ensemble forecasts with different starting times for maximum 2-metre temperature for the Polarstern location on 19 April.

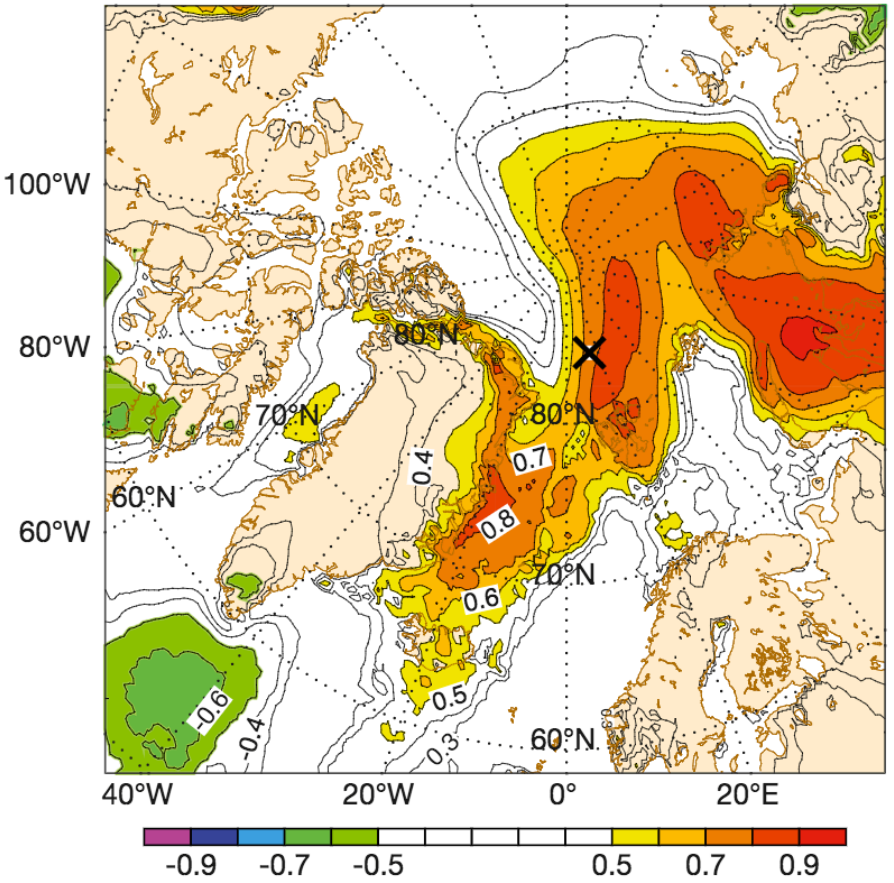

Two-metre maximum temperature EFI. The chart shows the 5-day forecast from 00 UTC on 15 April 2020 of the EFI for 2-metre maximum temperature on 19 April.

Results on site of ECMWF

In particular

T. Haiden *et al.*, 2021, *Evaluation of ECMWF forecasts, including the 2020 upgrade*, Technical Memorandum 880, ECMWF, Reading, UK.

Available at the address :

https://www.ecmwf.int/en/elibrary/19879-evaluation-ecmwf-forecasts-including-2020-upgrade

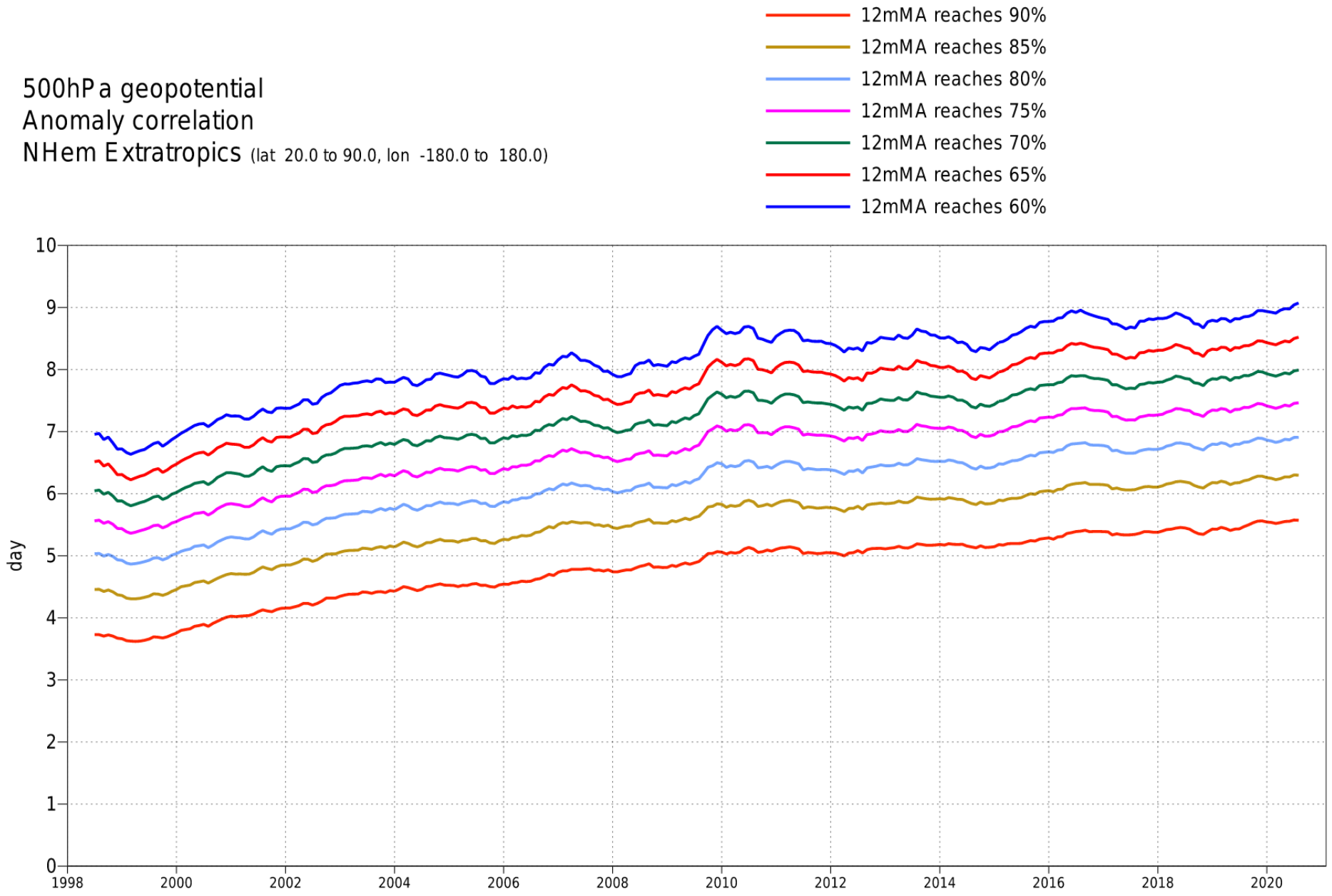

Lead time ACC reaching thresholds

Spatial correlation between anomalies from climatology of forecast and verifying analysis

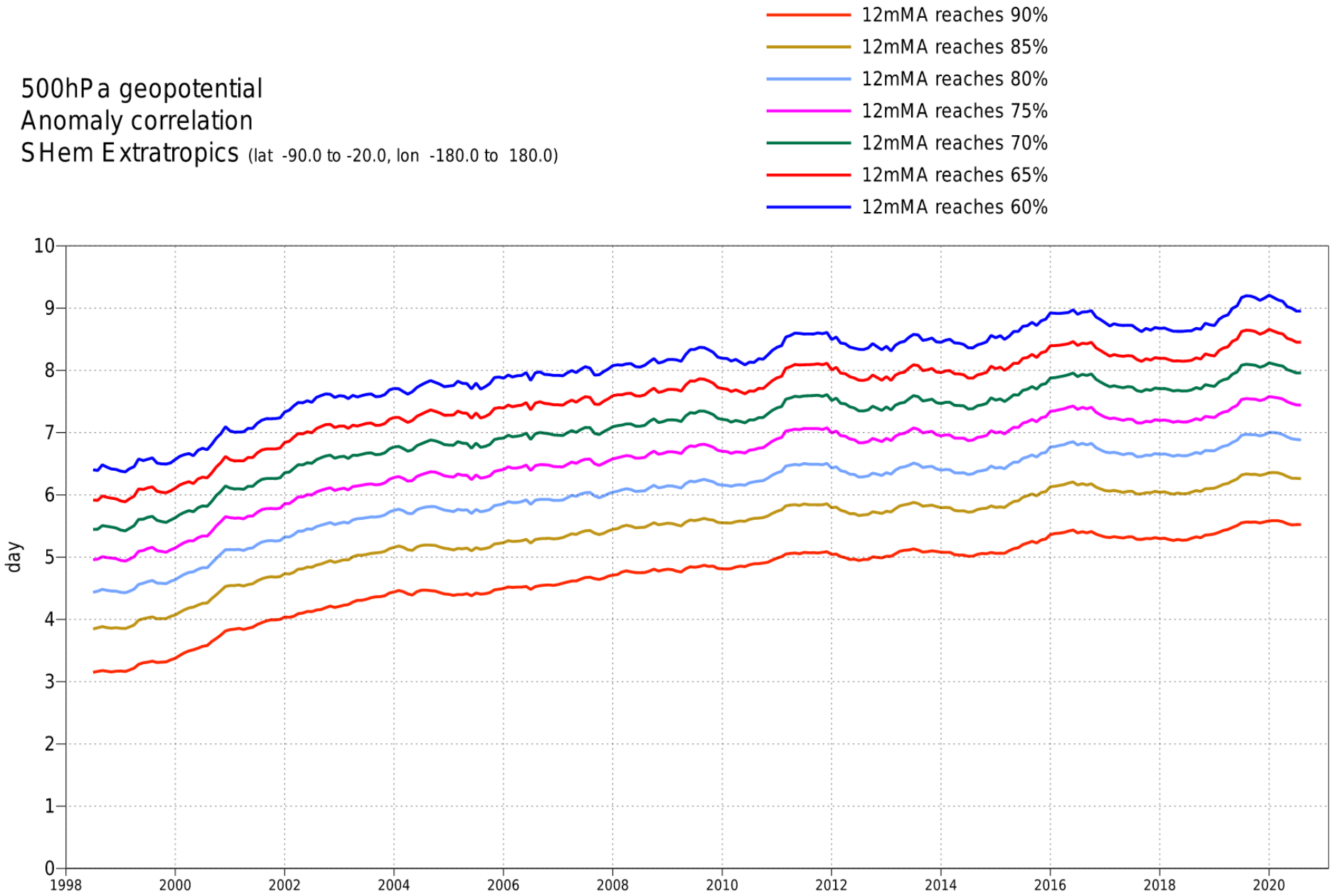

Lead time ACC reaching thresholds

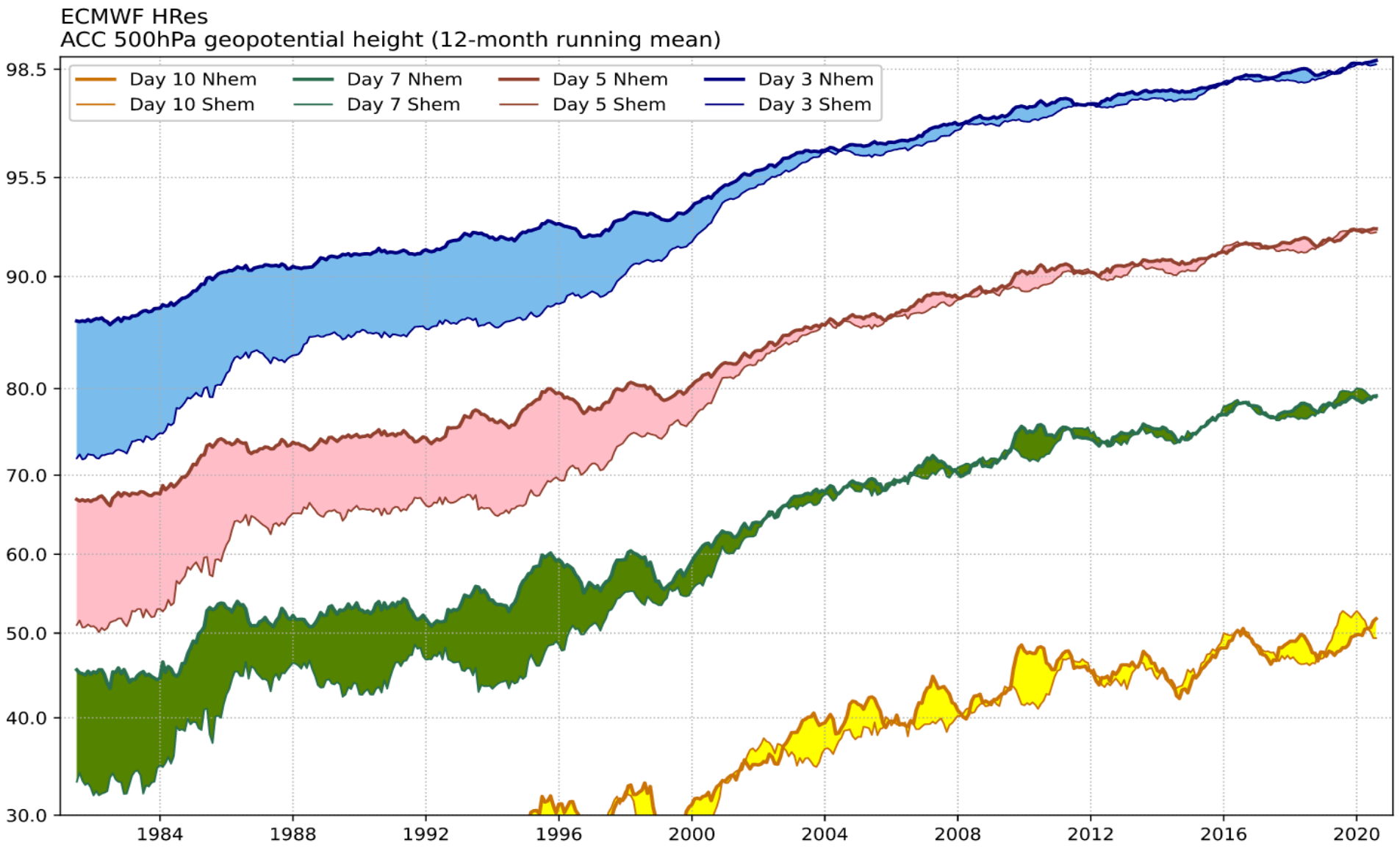
ECMWF HRes
ACC 500hPa geopotential height (12-month running mean)
Day 10 Nhem
Day 10 Shem
Day 7 Nhem
Day 7 Shem
Day 5 Nhem
Day 5 Shem
Day 3 Nhem
Day 3 Shem
98.5
95.5
90.0
80.0
70.0
60.0
50.0
40.0
30.0
1984
1988
1992
1996
2000
2004
2008
2012
2016
2020

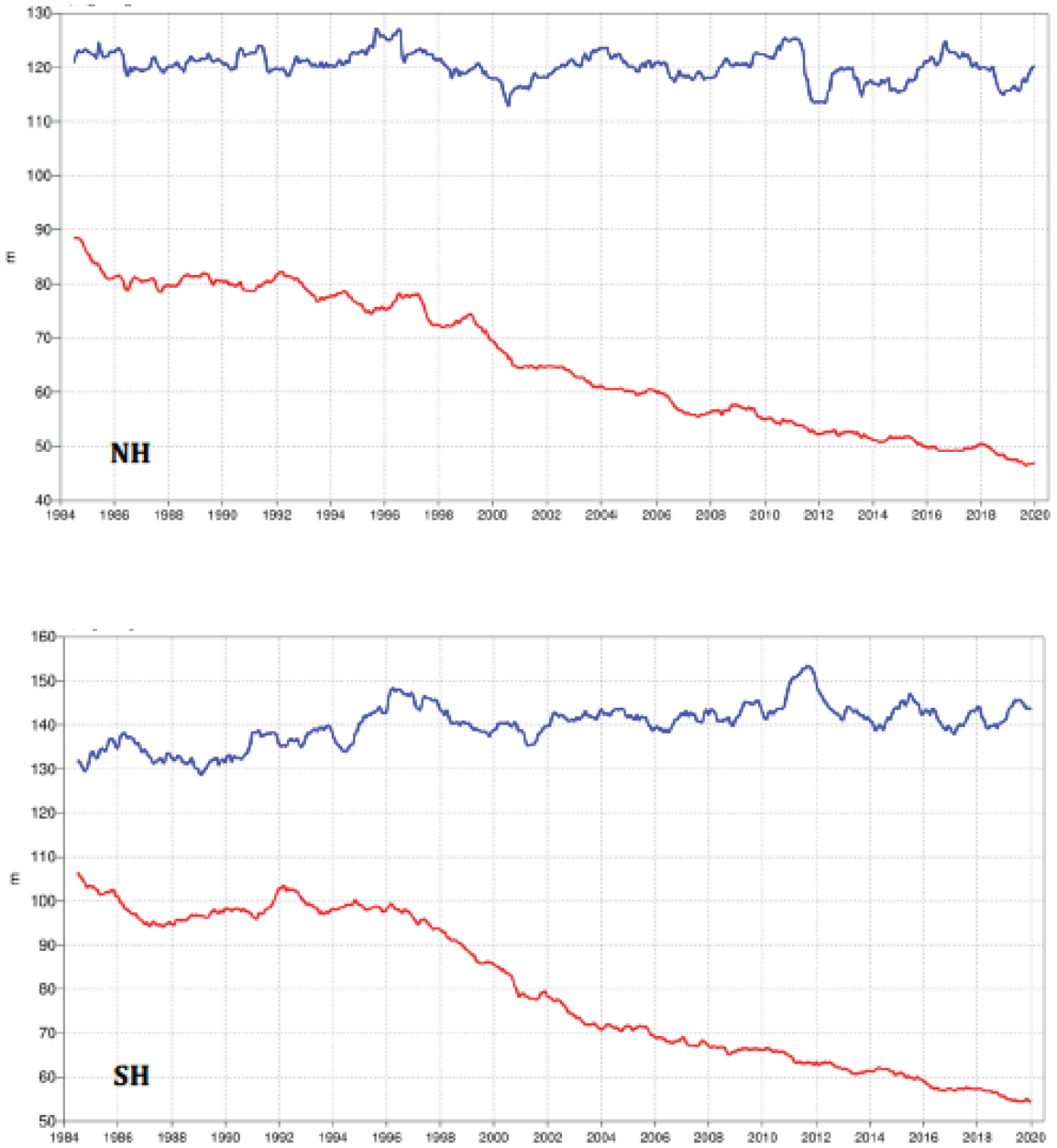

Figure 4: Root mean square (RMS) error of forecasts of 500 hPa geopotential height (m) at day 6 (red), verified against analysis. For comparison, a reference forecast made by persisting the analysis over 6 days is shown (blue). Plotted values are 12-month moving averages; the last point on the curves is for the 12-month period August 2019–July 2020. Results are shown for the northern extra-tropics (top), and the southern extra-tropics (bottom).

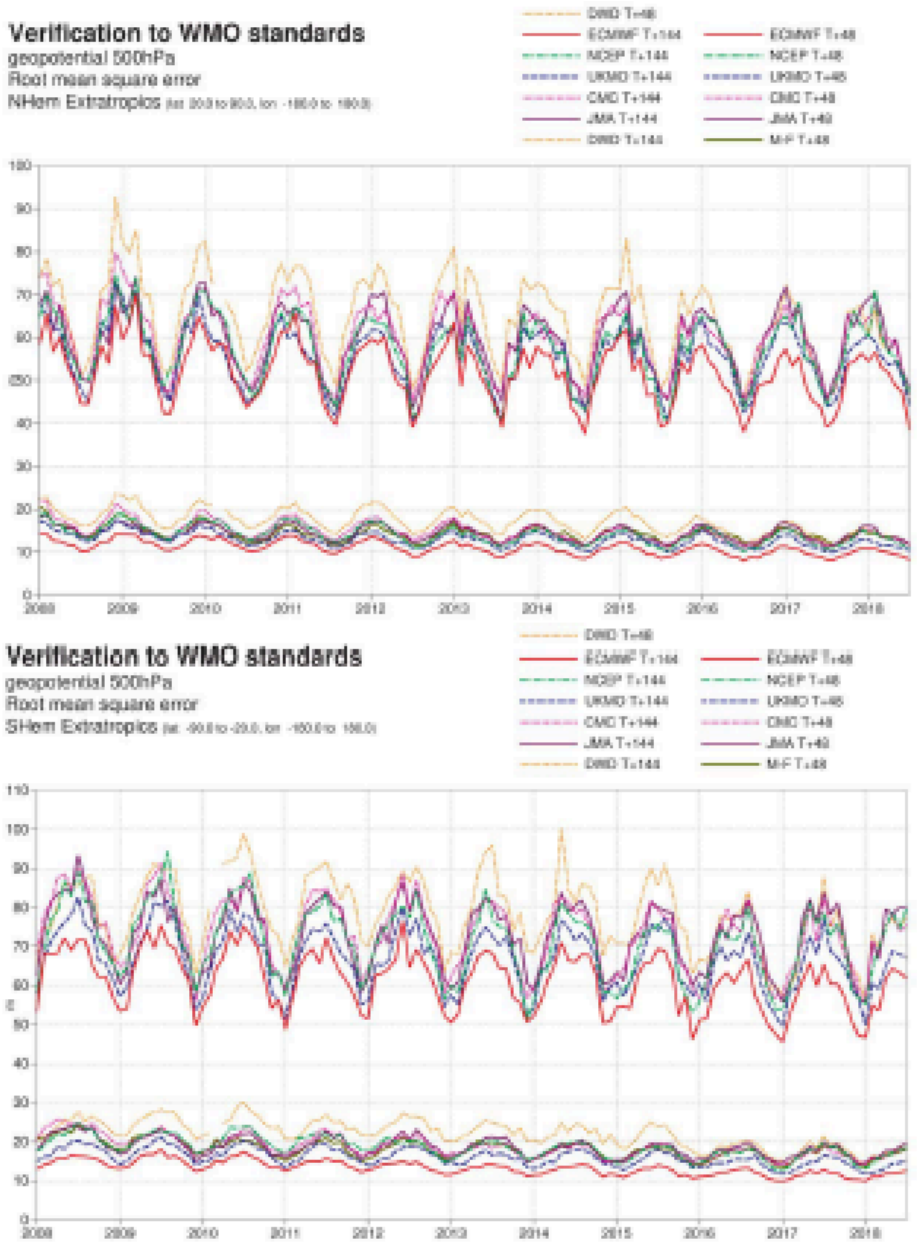

2020

Figure 14: WMO-exchanged scores from global forecast centres. RMS error of 500 hPa geopotential height over northern (top) and southern (bottom) extratropics. In each panel, the upper curves show the six-day forecast error and the lower curves show the two-day forecast error of model runs initiated at 12 UTC. Each model is verified against its own analysis. JMA = Japan Meteorological Agency, CMC = Canadian Meteorological Centre, UKMO = the UK Met Office, NCEP = U.S. National Centers for Environmental Prediction, M-F = Météo France, DWD = Deutscher Wetterdienst.

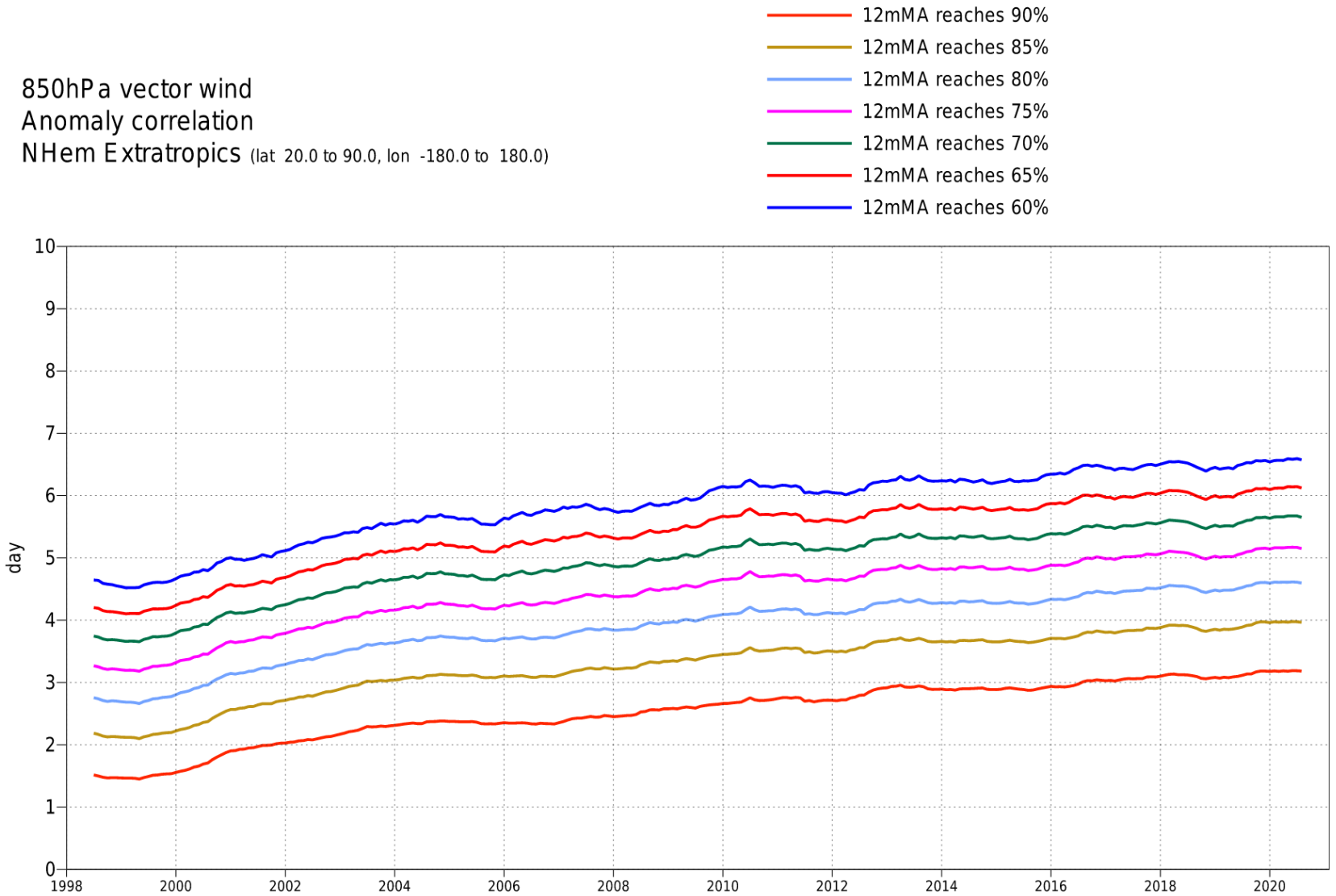

Lead time ACC reaching thresholds

Spatial correlation between anomalies from climatology of forecast and verifying analysis

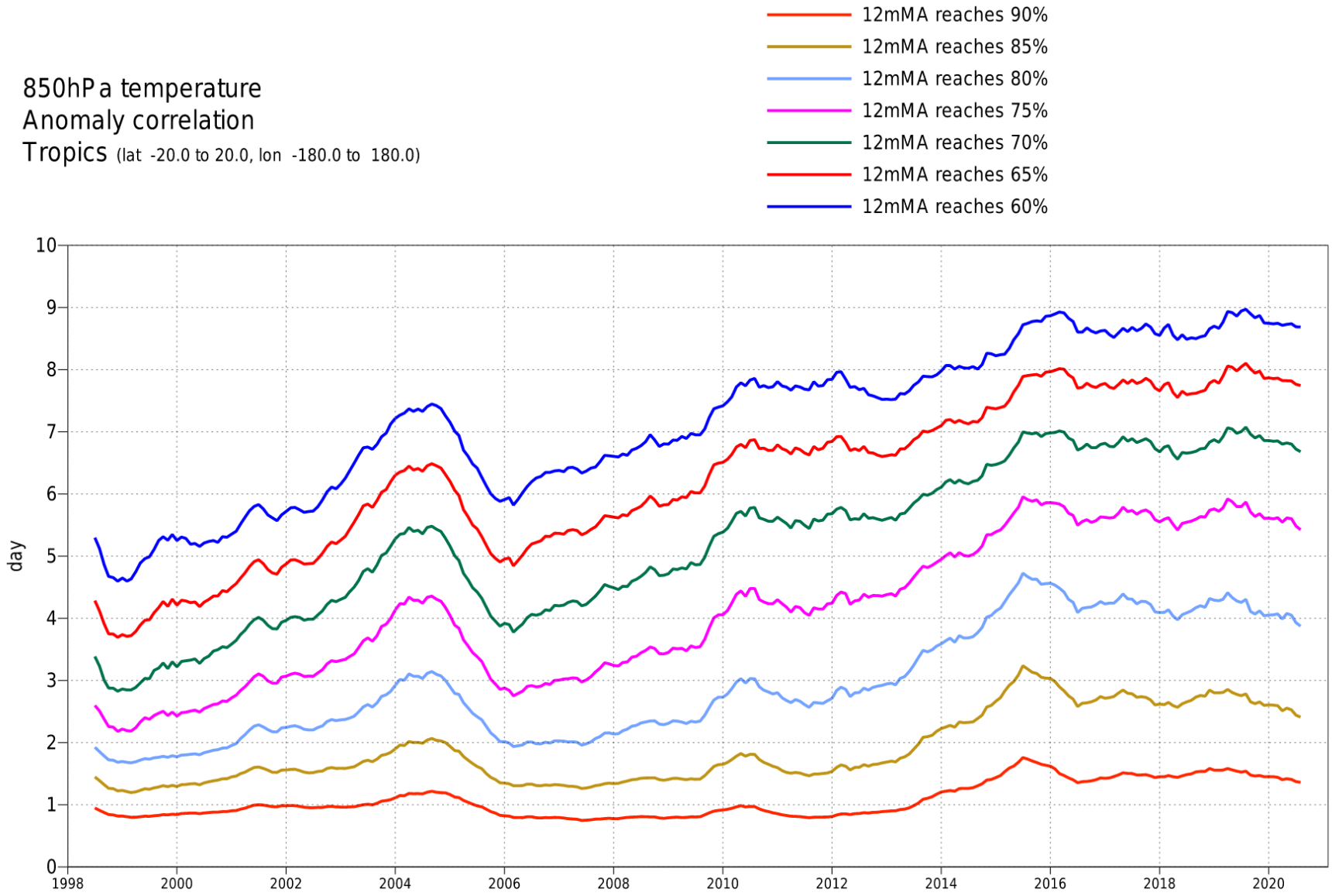

Lead time ACC reaching thresholds

Spatial correlation between anomalies from climatology of forecast and verifying analysis

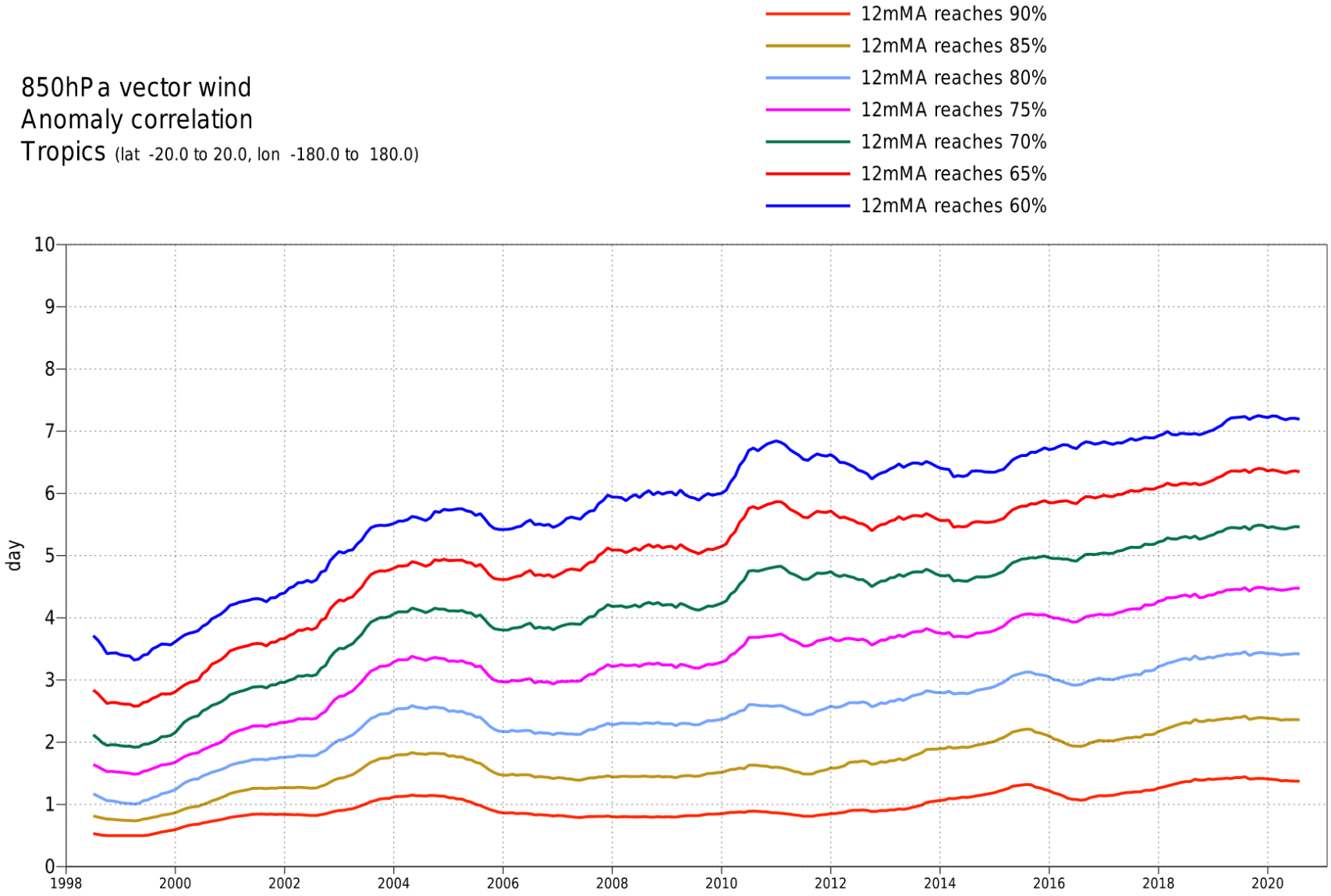

Lead time ACC reaching thresholds

Spatial correlation between anomalies from climatology of forecast and verifying analysis

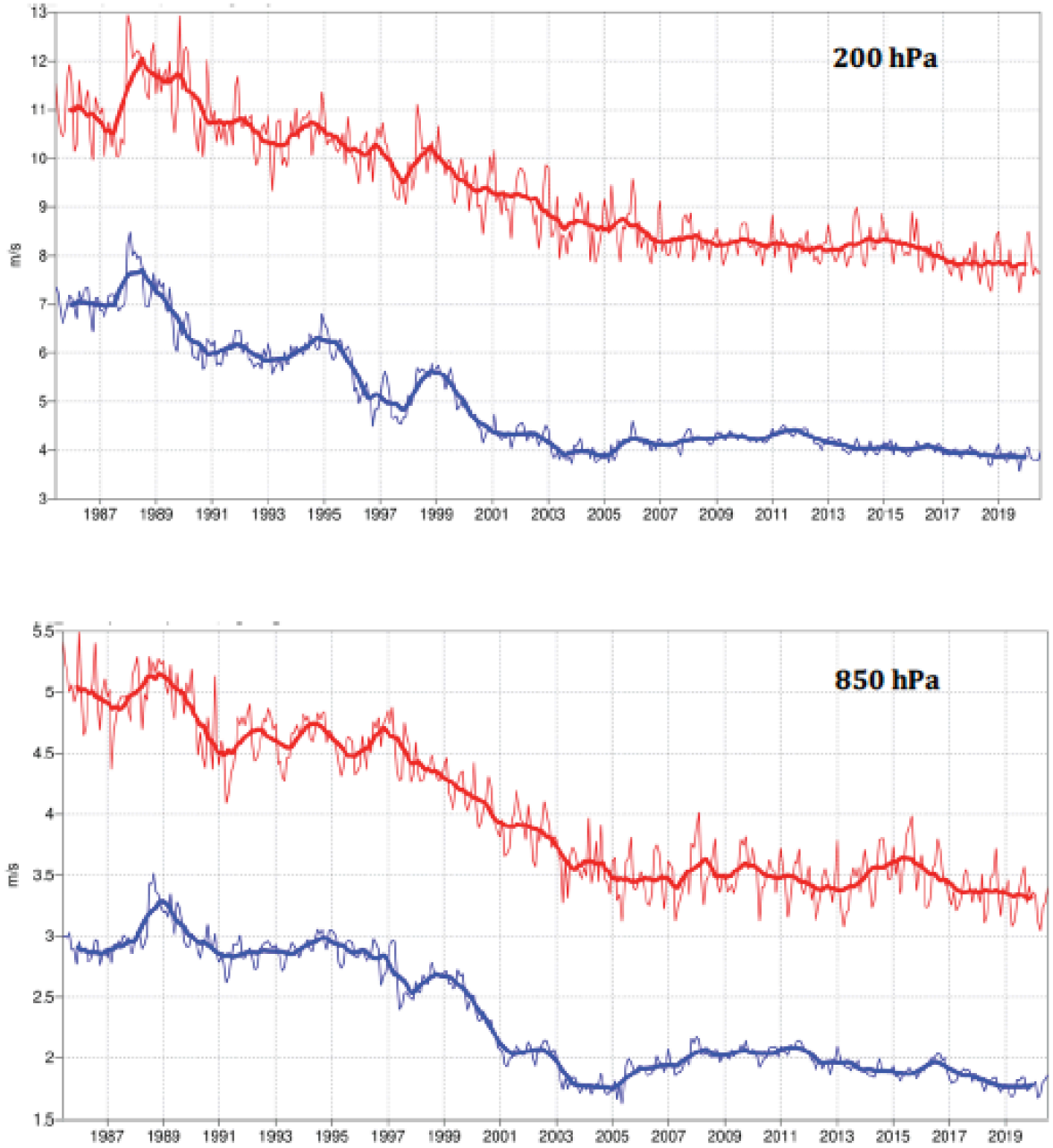

Figure 12: Forecast performance in the tropics. Curves show the monthly average RMS vector wind|errors at 200 hPa (top) and 850 hPa (bottom) for one-day (blue) and five-day (red) forecasts, verified against analysis. 12-month moving average scores are also shown (in bold).

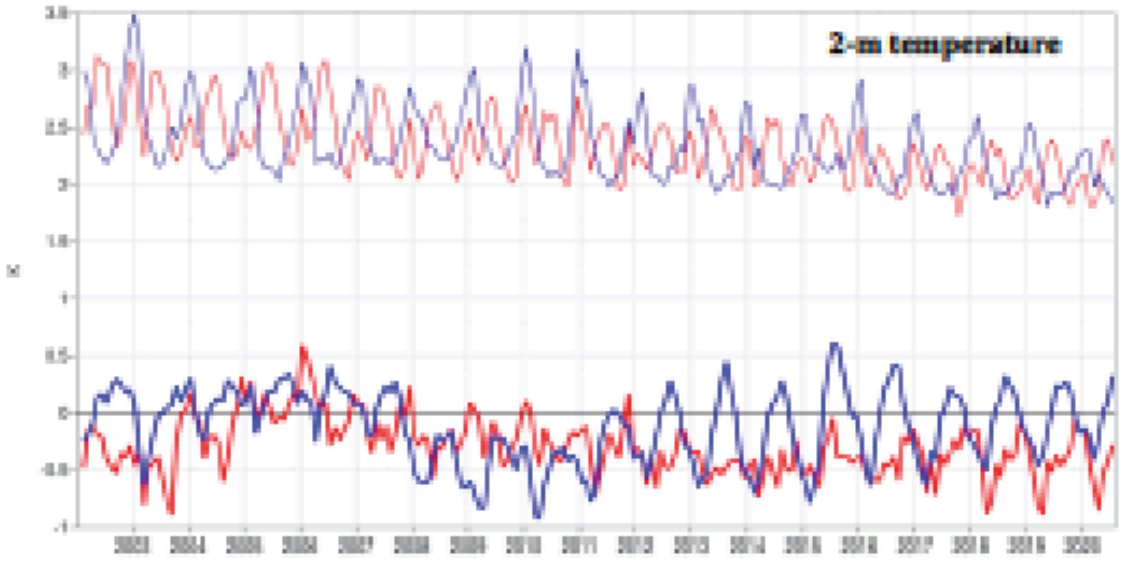

Figure 20: Verification of 2 m temperature forecasts against European SYNOP data on the GTS for 60-hour (night-time) and 72-hour (daytime) forecasts. Lower pair of curves shows bias, upper curves are standard deviation of error.

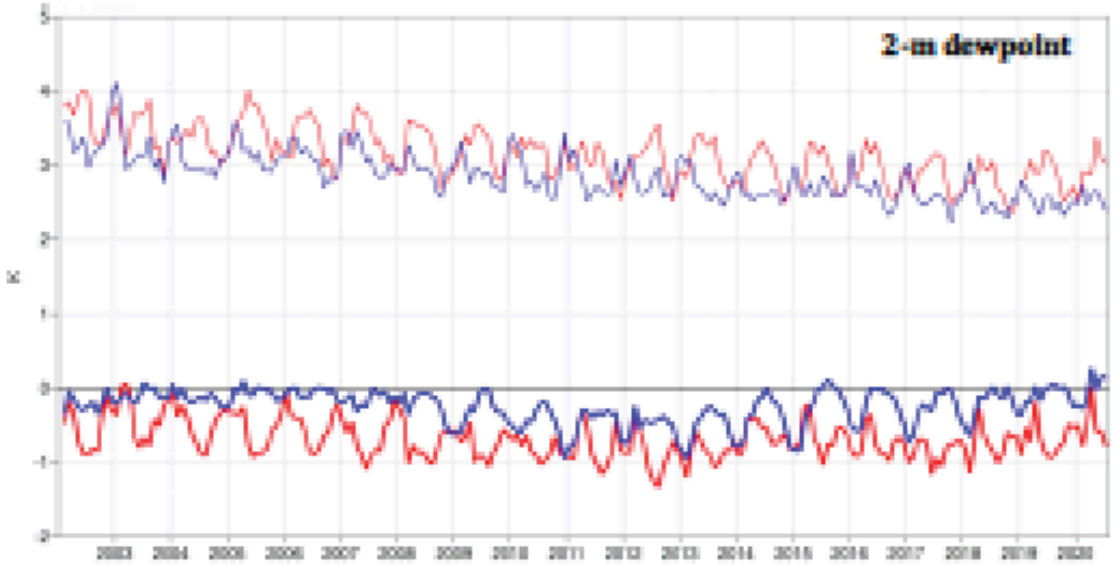

Figure 21: Verification of 2 m dew point forecasts against European SYNOP data on the Global Telecommunication System (GTS) for 60-hour (night-time) and 72-hour (daytime) forecasts. Lower pair of curves shows bias, upper curves show standard deviation of error.

Europe

Night time: blue curves
Day time: red curves

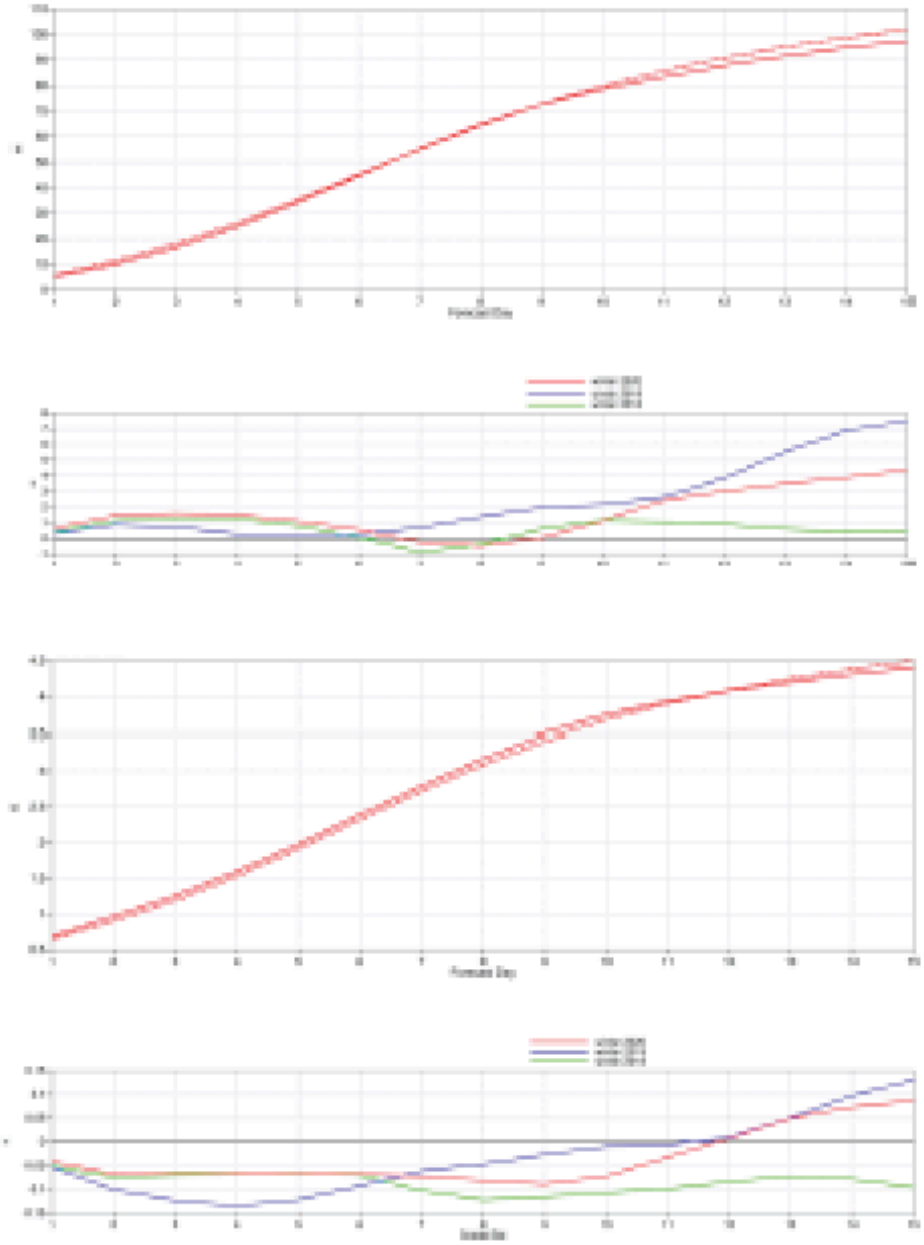

Figure 8: Ensemble spread (standard deviation, dashed lines) and RMS error of ensemble-mean (solid lines) for winter 2019–2020 (upper figure in each panel), and differences of ensemble spread and RMS error of ensemble mean for last three winter seasons (lower figure in each panel, negative values indicate spread is too small); verification is against analysis, plots are for 500 hPa geopotential (top) and 850 hPa temperature (bottom) over the extratropical northern hemisphere for forecast days 1 to 15.

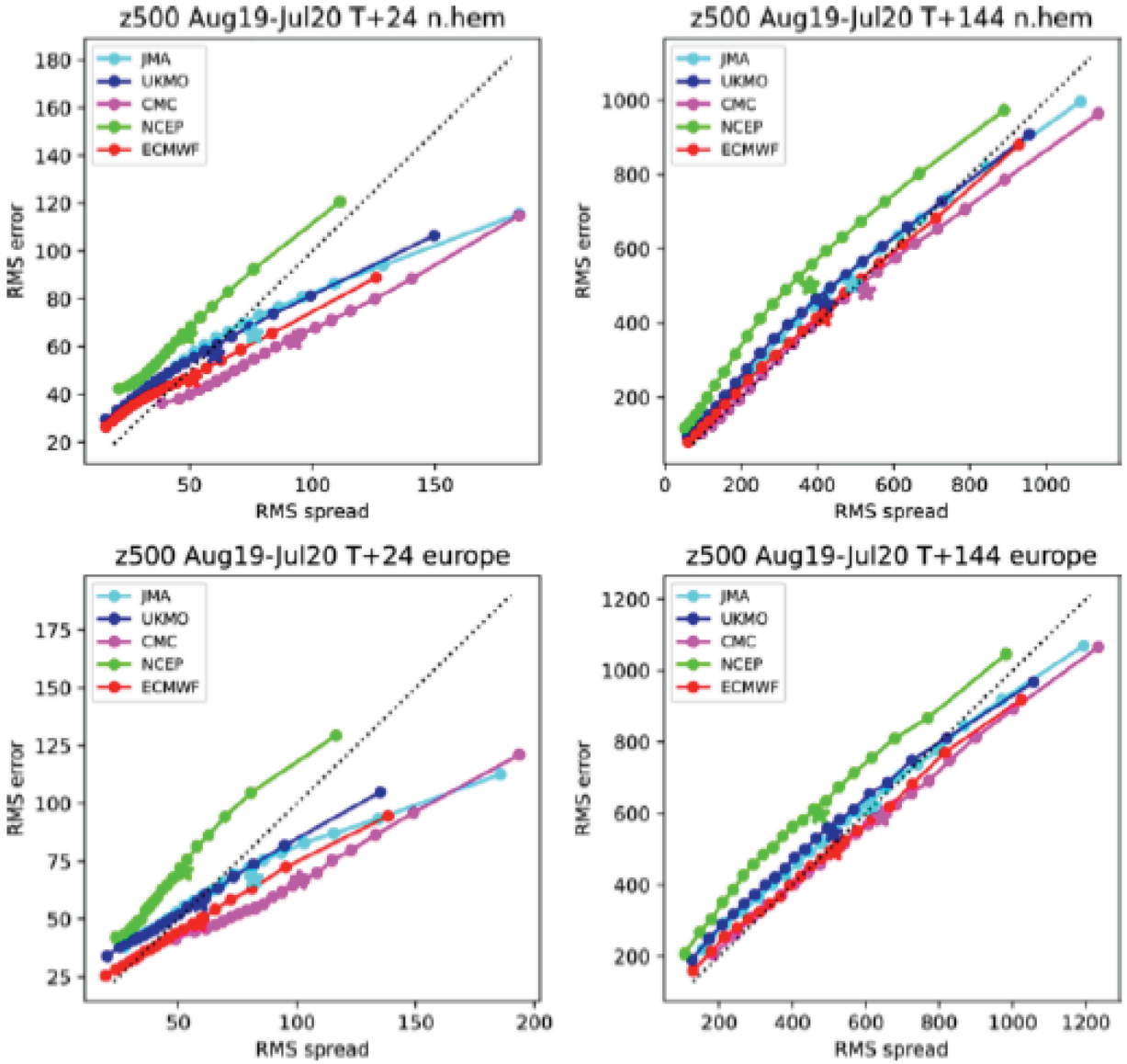

Figure 9: Ensemble spread reliability of different global models for 500 hPa geopotential for the period August 2019–July 2020 in the northern hemisphere extra-tropics (top) and in Europe (bottom) for day 1 (left) and day 6 (right), verified against analysis. Circles show error for different values of spread, stars show average error-spread relationship. Due to random outages in the data supply, NCEP curves are based on a reduced data set (70%).

Forecast day : 4, Parameter : 24h precipitation

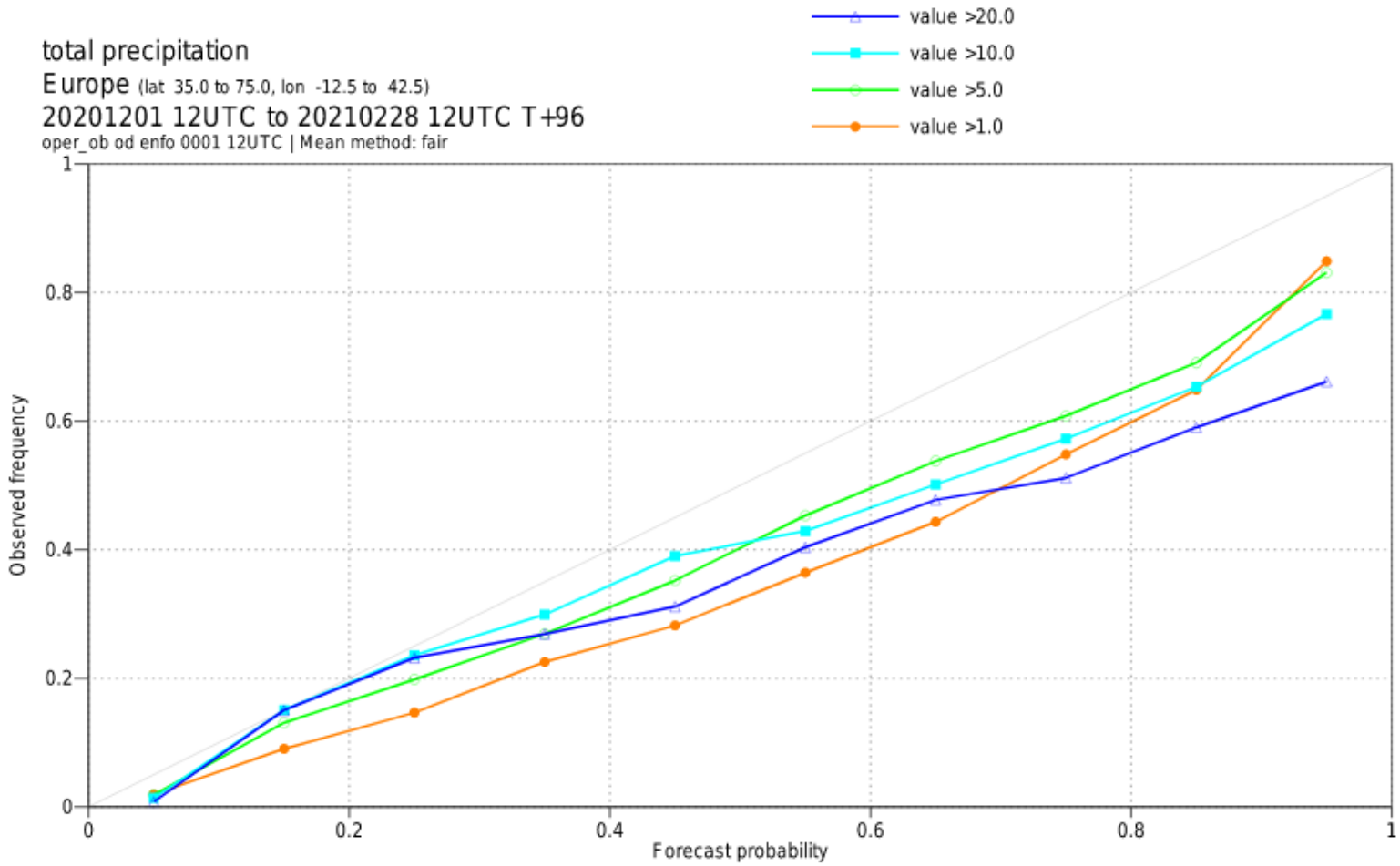

ECMWF

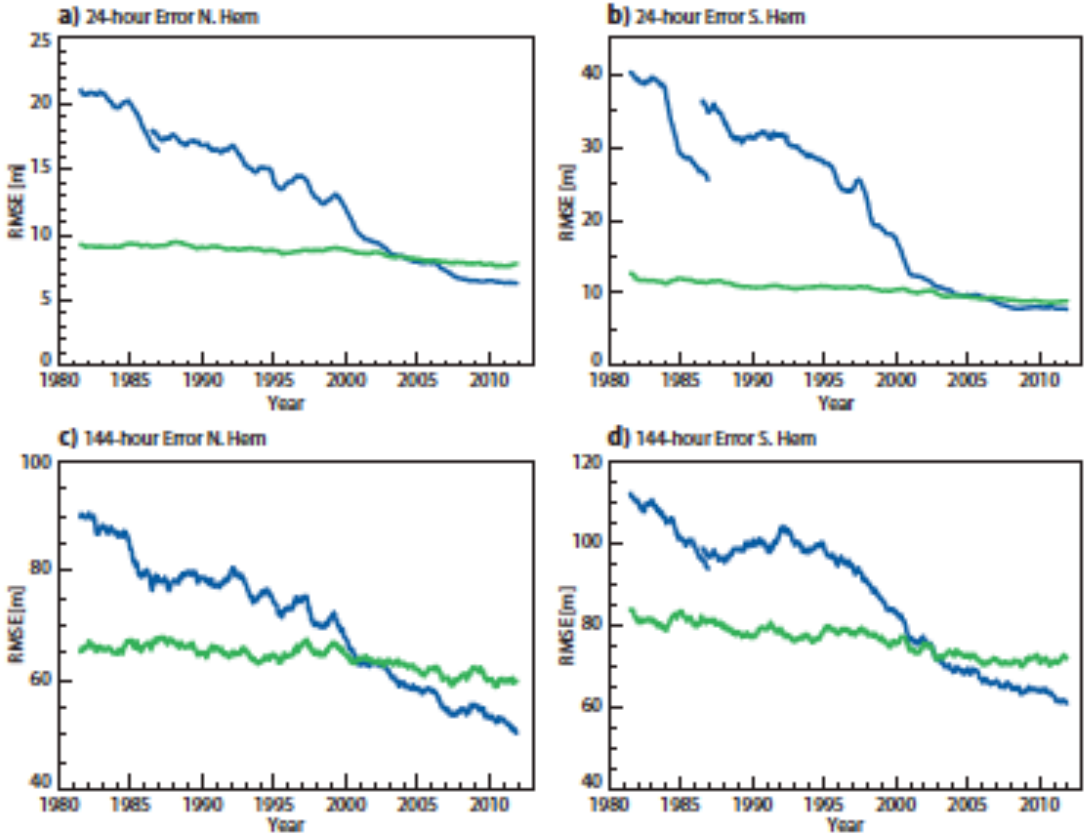

FIG. 3. Evolution of forecast errors from 1981 to 2012 for N.Hem (a and c) and S.Hem (b and d). Operational forecasts (blue) and ERA Interim (green). Note that before 1986 the operational analysis is used to verify the operational forecasts, after 1986 ERA Interim is used for the verification (with an overlap of 6 months present).

Remaining problems

- Water cycle (evaporation, condensation, influence on absorbed or emitted radiation)

- Exchanges with ocean or continental surface (heat, water, momentum, …)

- …

ECMWF data coverage (used observations) - SYNOP-SHIP-METAR
2021033121 to 2021040103
Total number of obs = 78182

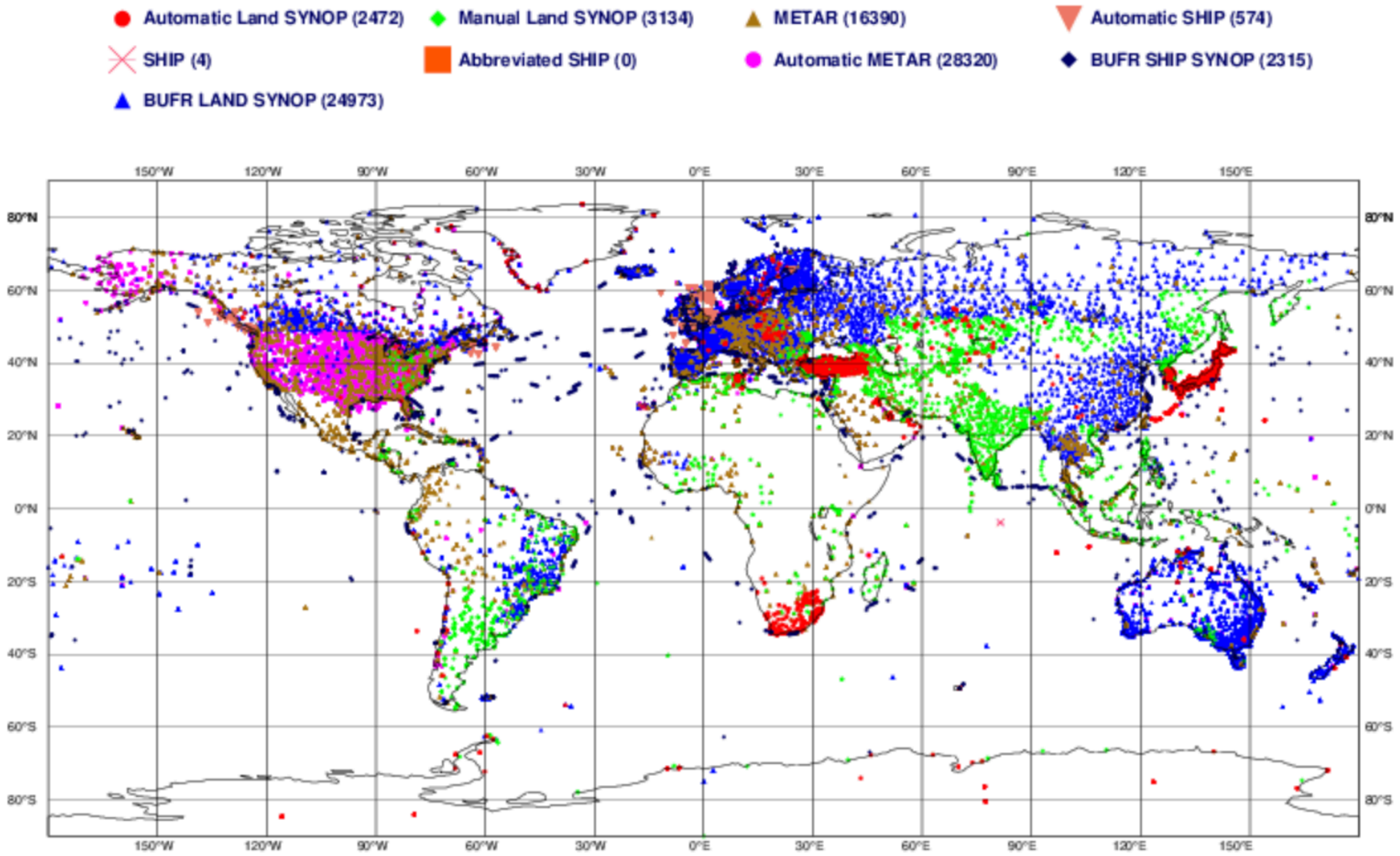

ECMWF data coverage (used observations) - RADIOSONDE
2021033121 to 2021040103
Total number of obs = 618

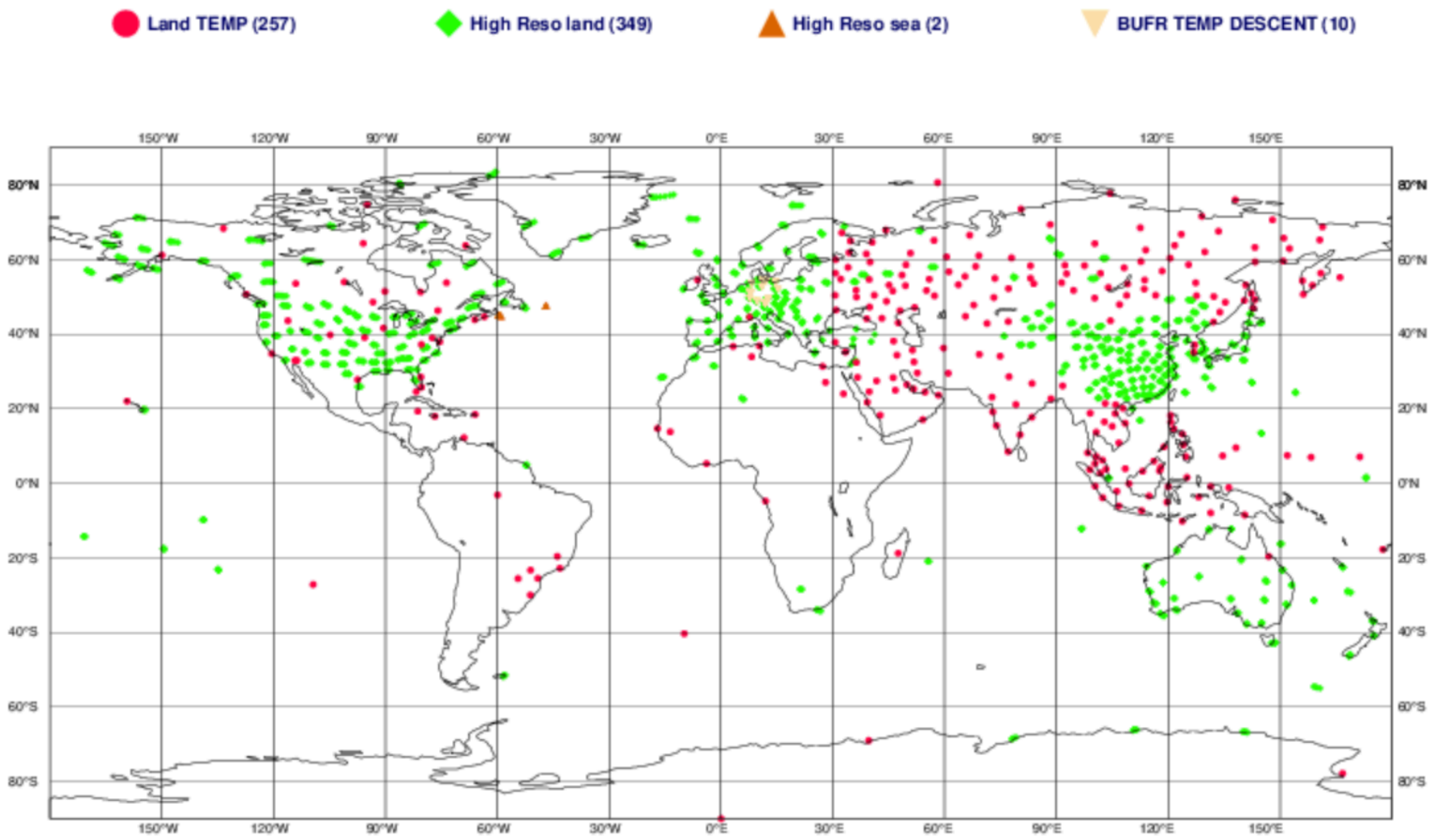

ECMWF data coverage (used observations) - AIRCRAFT
2021033121 to 2021040103
Total number of obs = 180186

AIREP (2142) | AMDAR (5447) | TAMDAR (3028) | WIGOS AMDAR (109373)

Mode-S (46145) | ADS-C (9295) | AFIRS (4756)

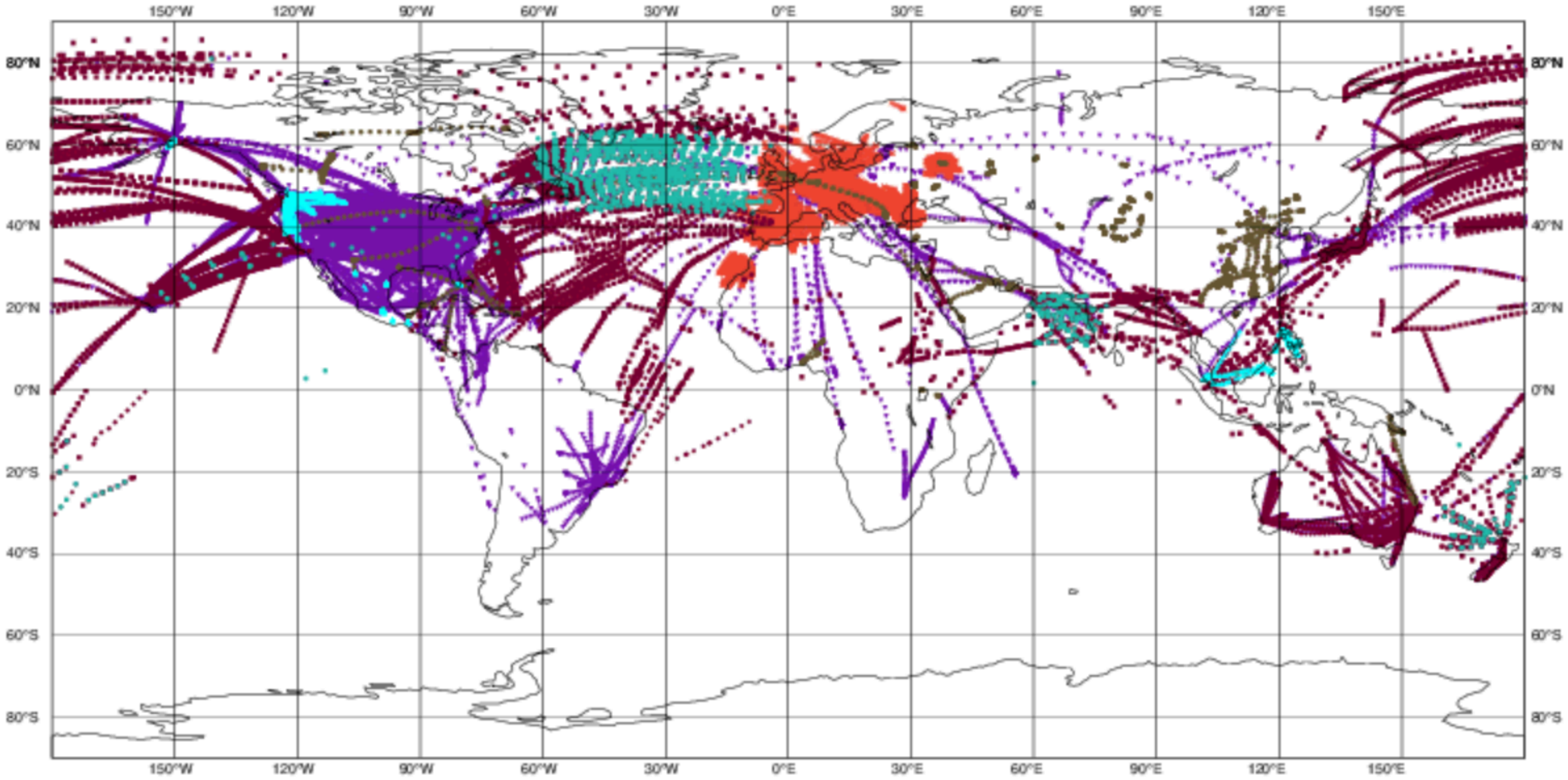

ECMWF data coverage (used observations) - AMSUA
2021033121 to 2021040103
Total number of obs = 76158

NOAA-15 (12423) NOAA-18 (8852) NOAA-19 (13397) METOP-A (12845)

METOP-B (15680) METOP-C (12961)

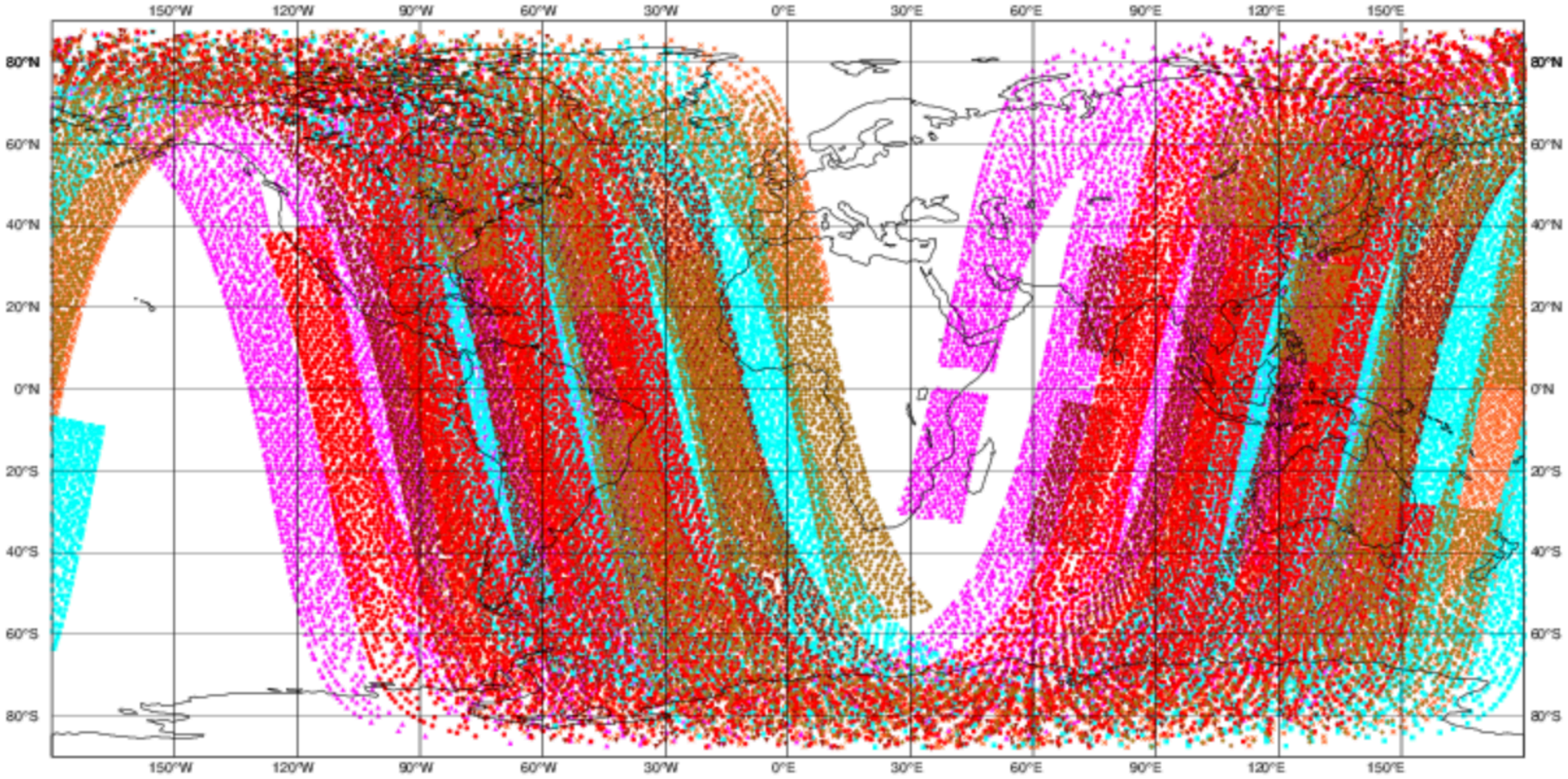

ECMWF data coverage (used observations) - IASI
2021033121 to 2021040103
Total number of obs = 35313

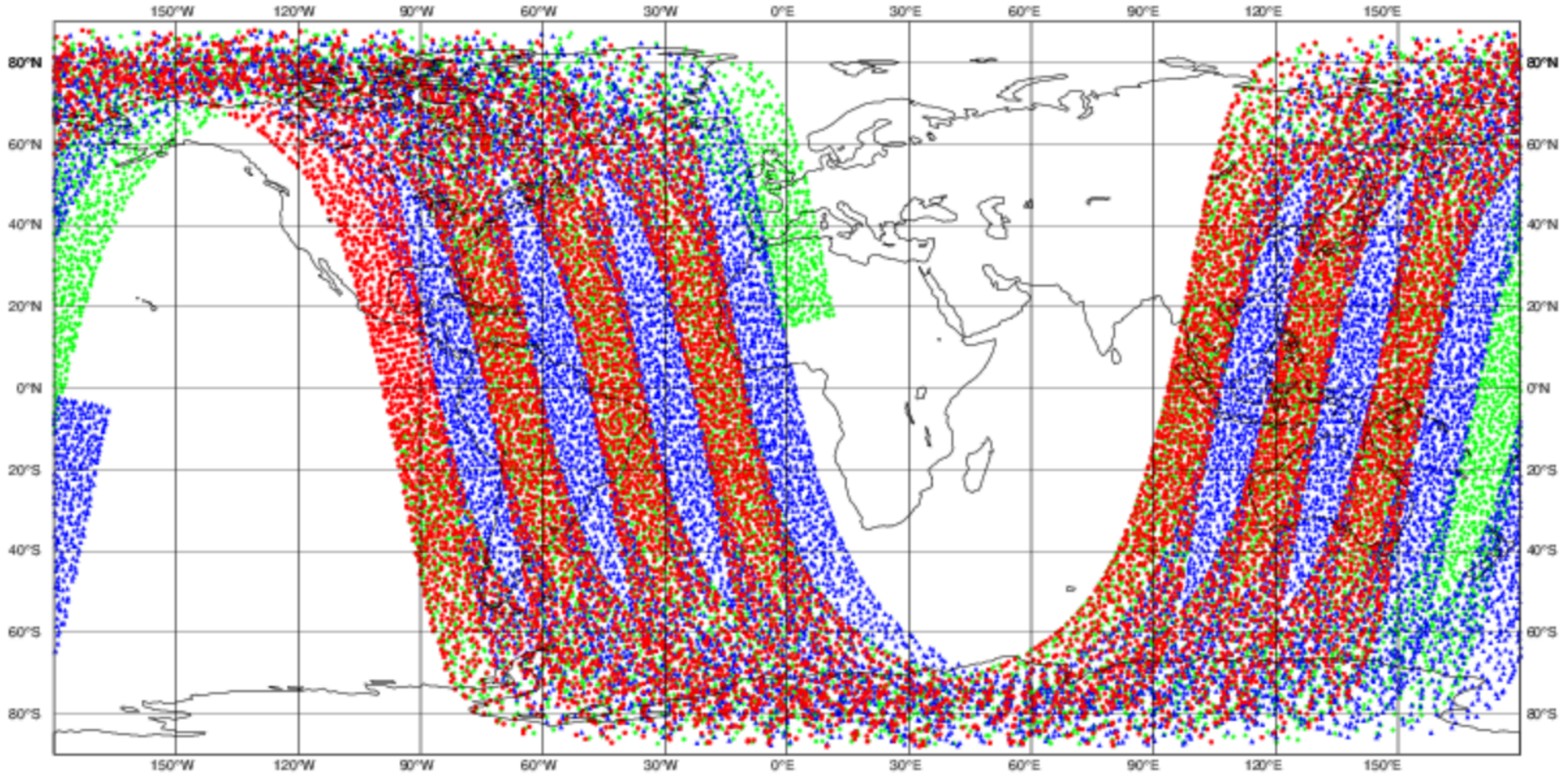

ECMWF data coverage (used observations) - AMV WV
2021033121 to 2021040103
Total number of obs = 31607

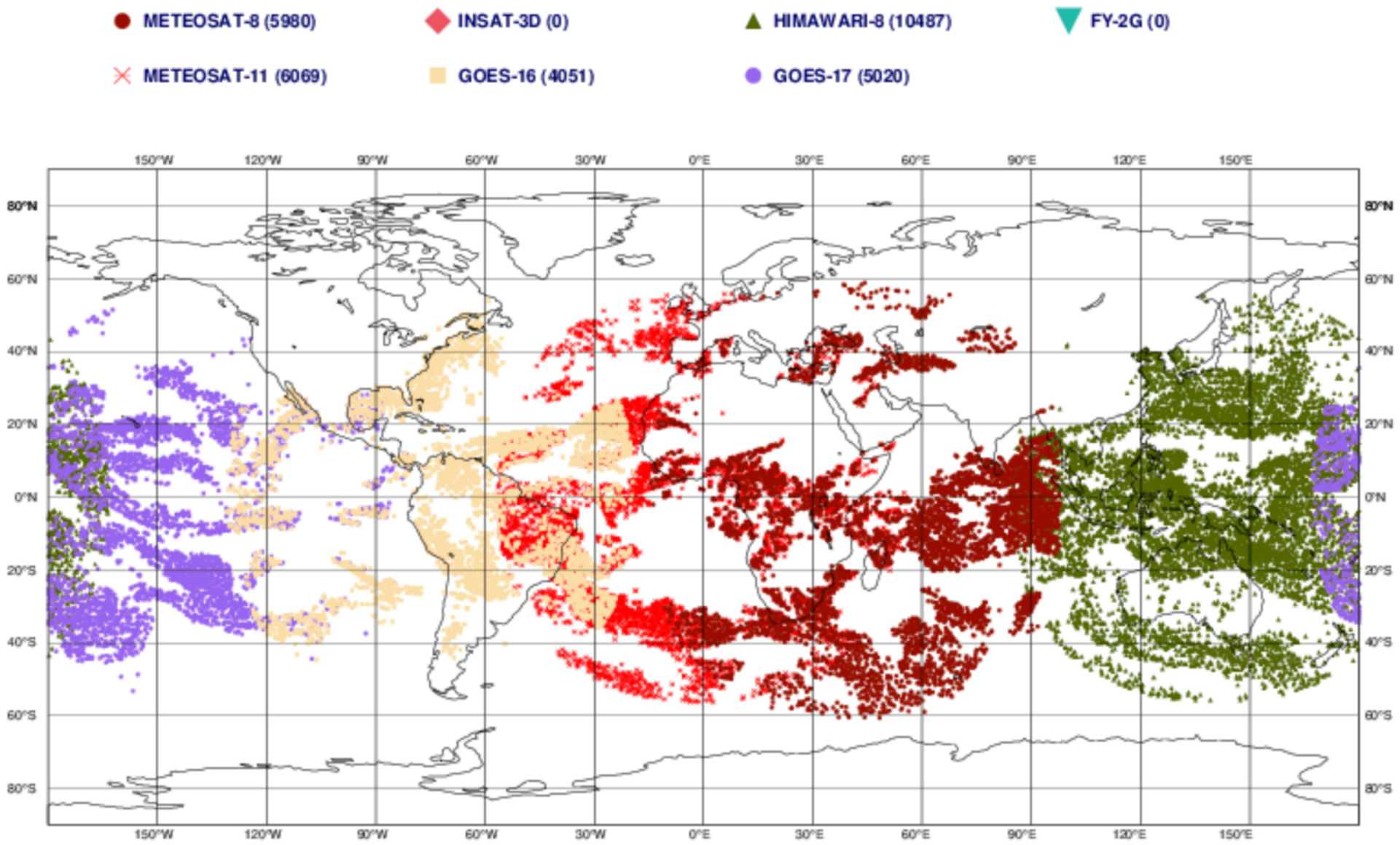

ECMWF data coverage (used observations) - GPSRO
2021033121 to 2021040103
Total number of obs = 33803

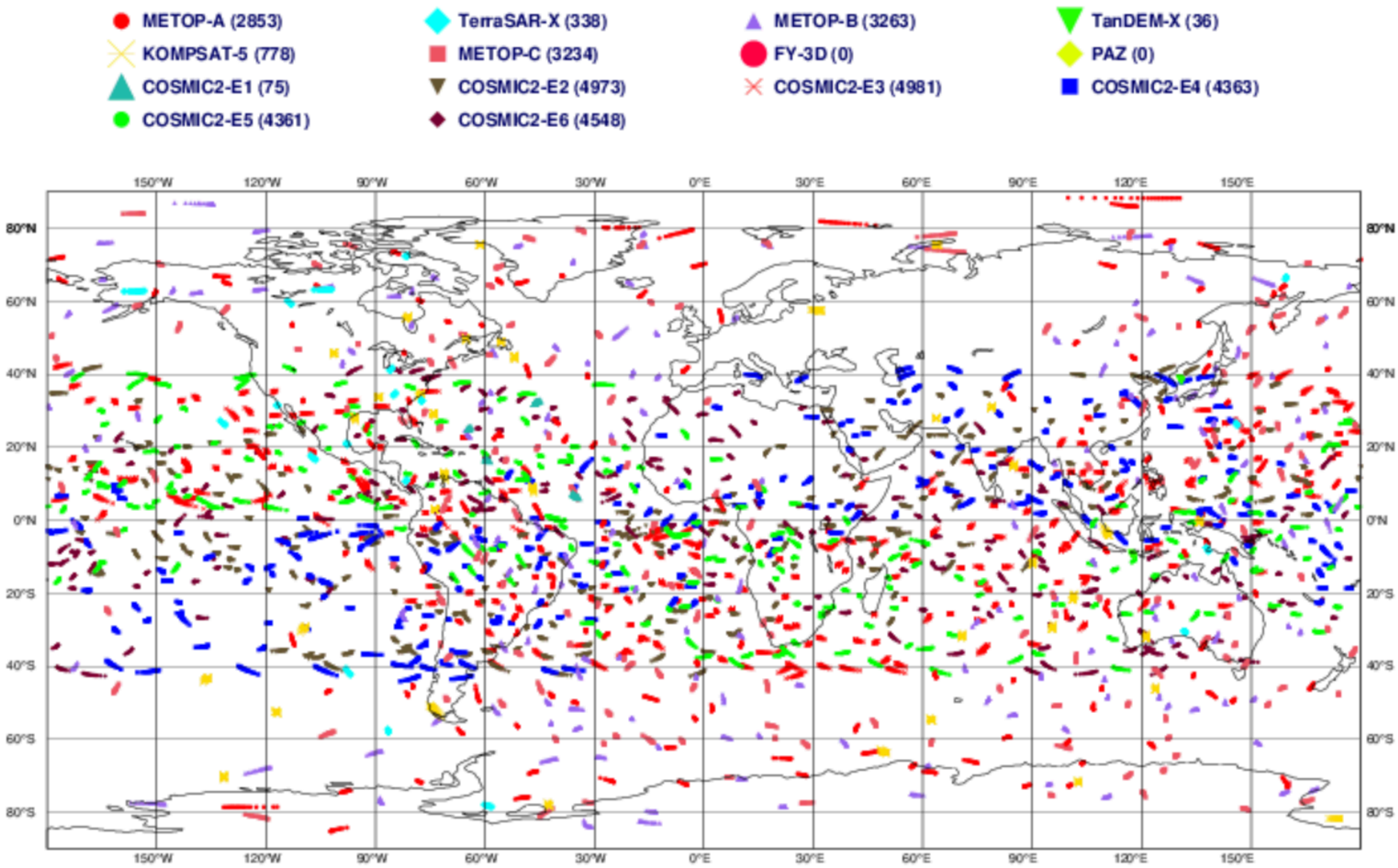

Satellite **ADM-Aeolus** was launched on August 22 2018. It carries a Lidar-Doppler instrument, called Aladin (Atmospheric LAser Doppler Instrument), that makes side measurements of wind in the volume of the atmosphere. Preliminary tests have shown that these new observations have a positive impact on the quality of the previsions, especially in the tropics and in the Southern Hemisphere. Aladin observations are now used operationally at ECMWF

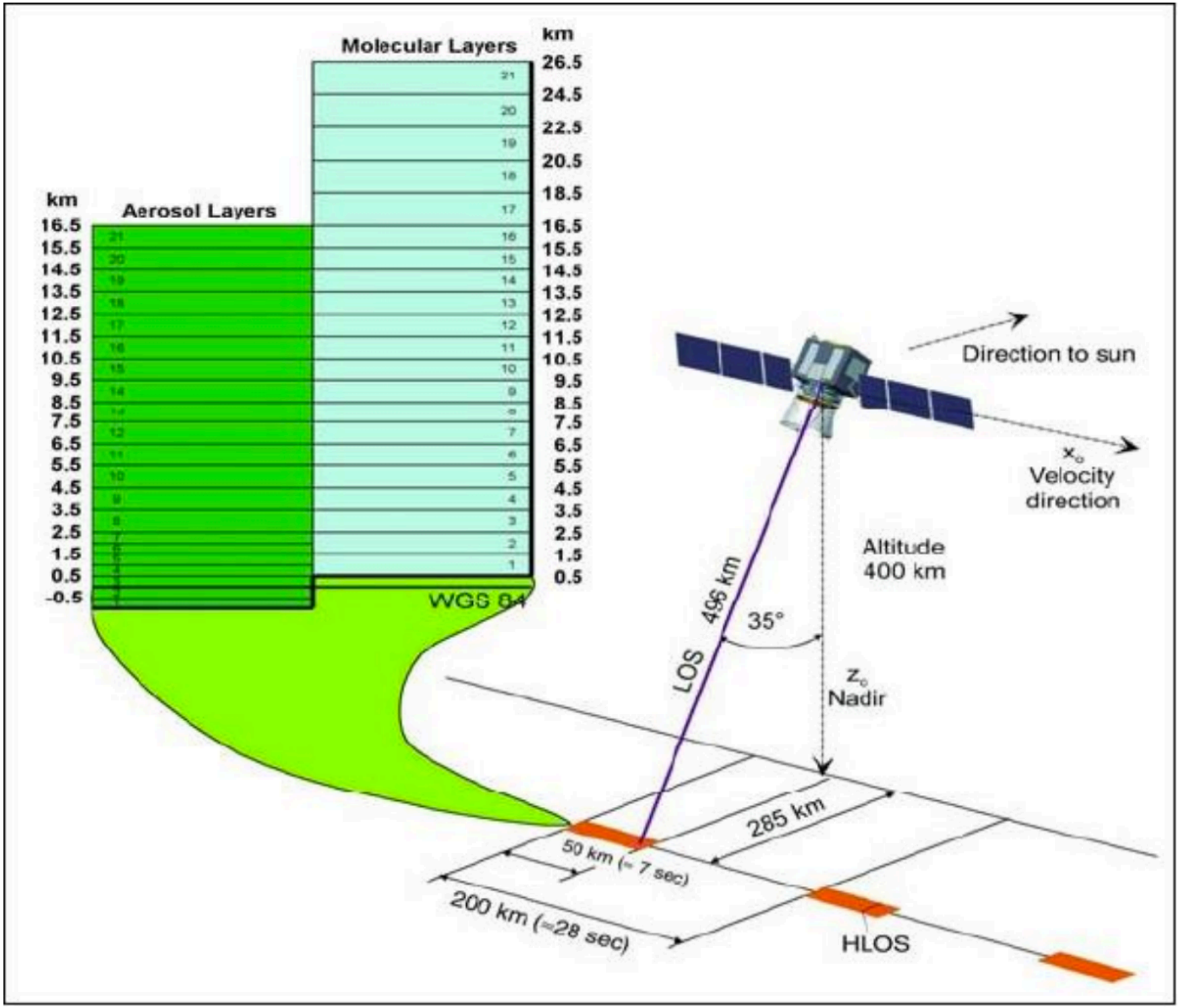

Figure 21: The ADM-Aeolus measurement and sampling concept (image credit: ESA)

ECMWF

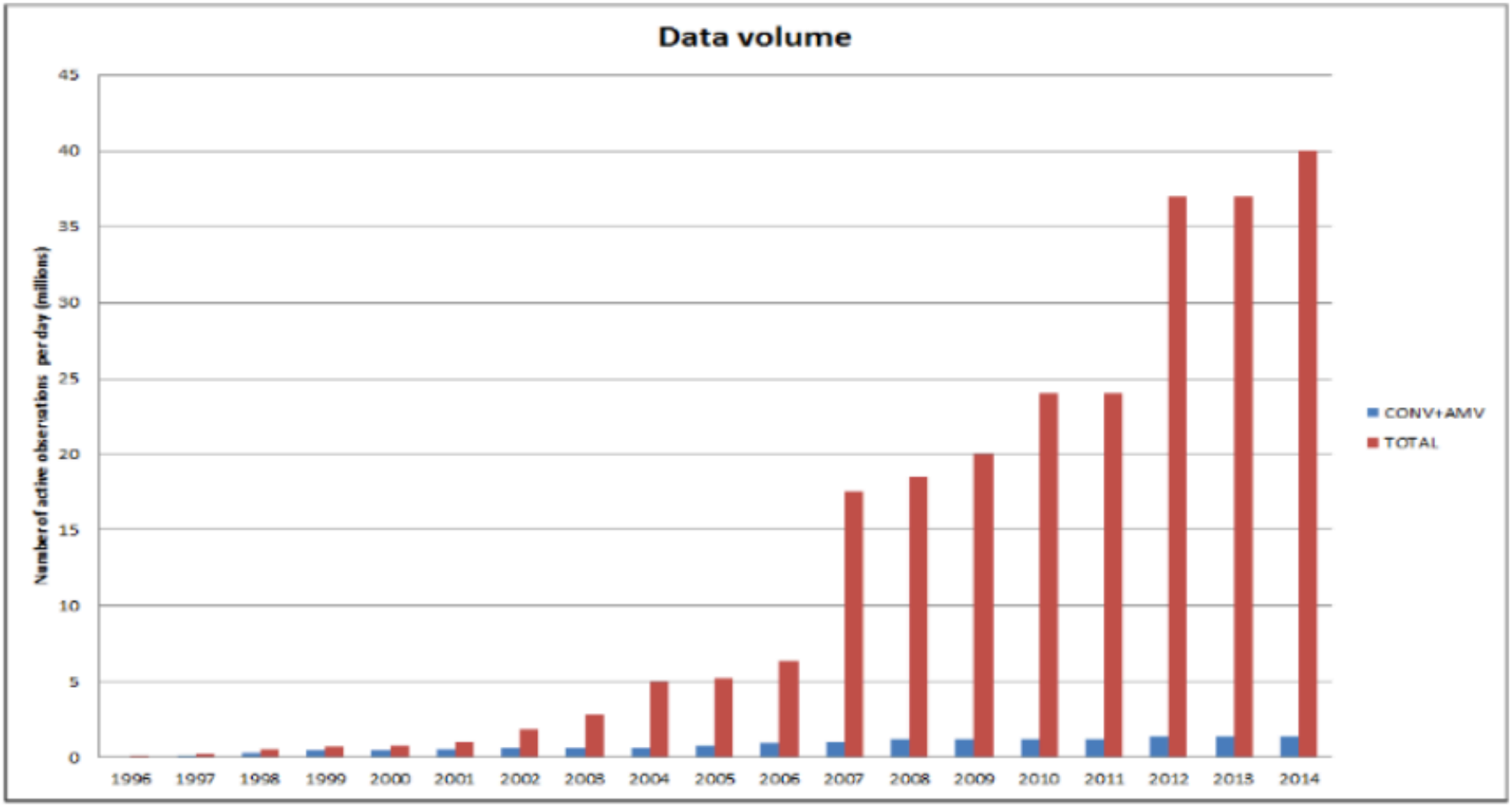
Data volume
Number of active observations per day (millions)
45
40
35
30
25
20
15
10
5
0
1996
1997
1998
1999
2000
2001
2002
2003
2004
2005
2006
2007
2008
2009
2010
2011
2012
2013
2014
CONV+AMV
TOTAL

- *Synoptic* observations (ground observations, radiosonde observations), performed simultaneously, by international agreement, in all meteorological stations around the world (00:00, 06:00, 12:00, 18:00 UTC)

- *Asynoptic* observations (satellites, aircraft), performed more or less continuously in time.

- *Direct* observations (temperature, pressure, horizontal components of the wind, moisture), which are local and bear on the variables used for describing the flow in numerical models.

- *Indirect* observations (radiometric observations, …), which bear on some more or less complex combination (most often, a one-dimensional spatial integral) of variables used for for describing the flow

$$y = H(\boldsymbol{x})$$

H : *observation operator (*for instance, radiative transfer equation)

ECMWF data coverage (used observations) - SEA LEVEL ANOMALY
20210330 00
Total number of obs = 4824

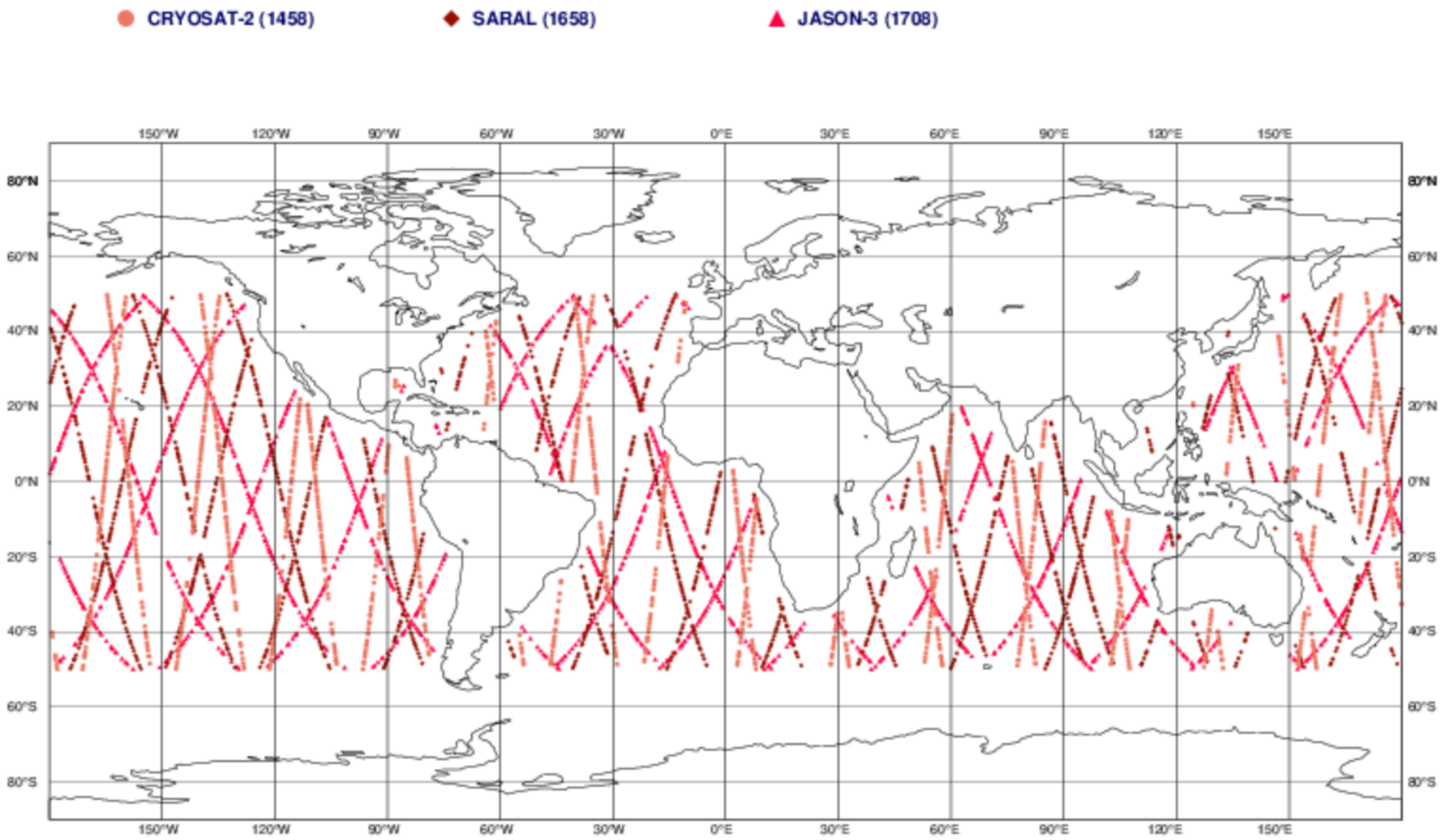

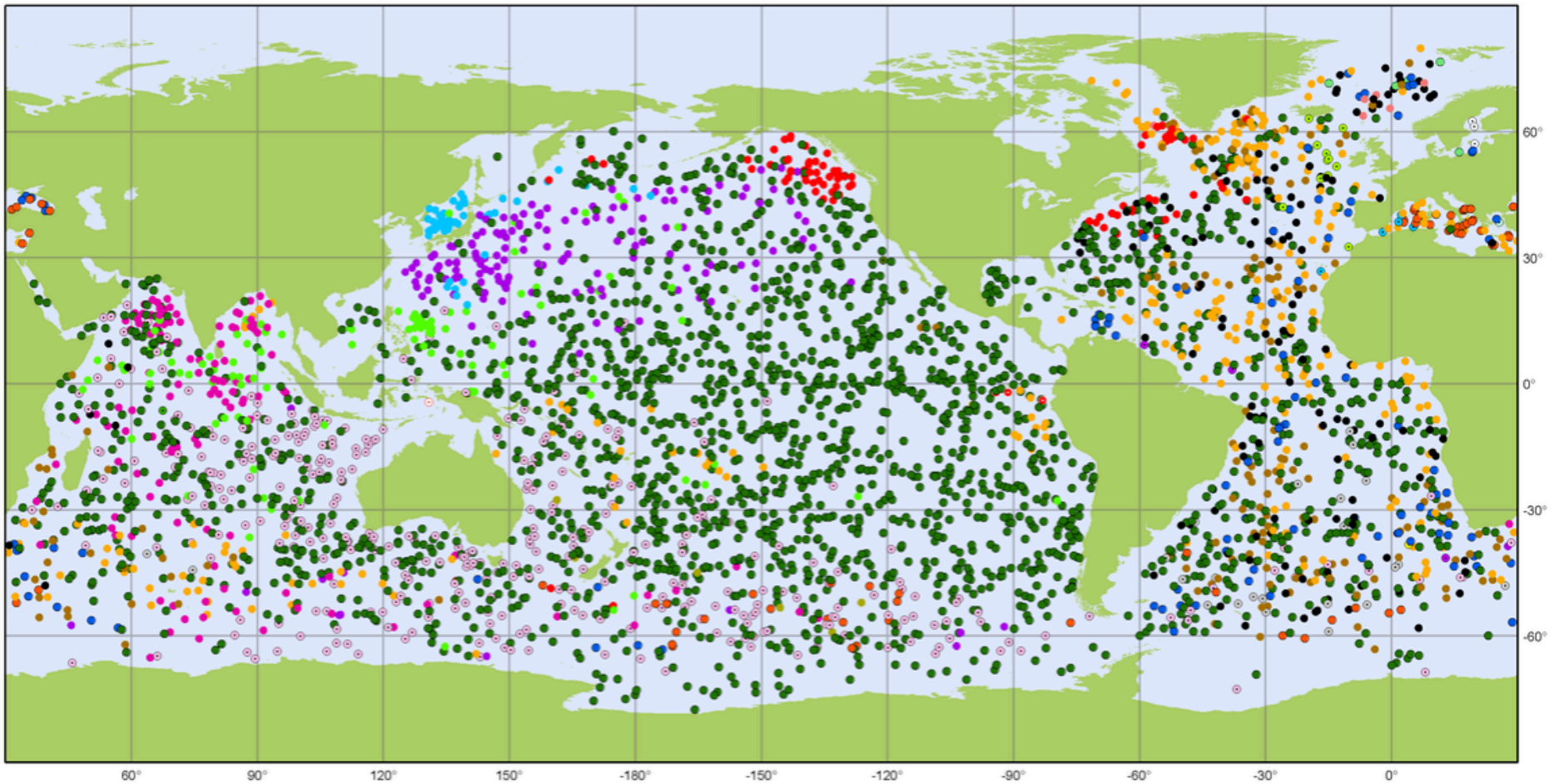

Argo **National contributions - 3881 Operational Floats** **February 2018**

Latest location of operational floats (data distributed within the last 30 days)

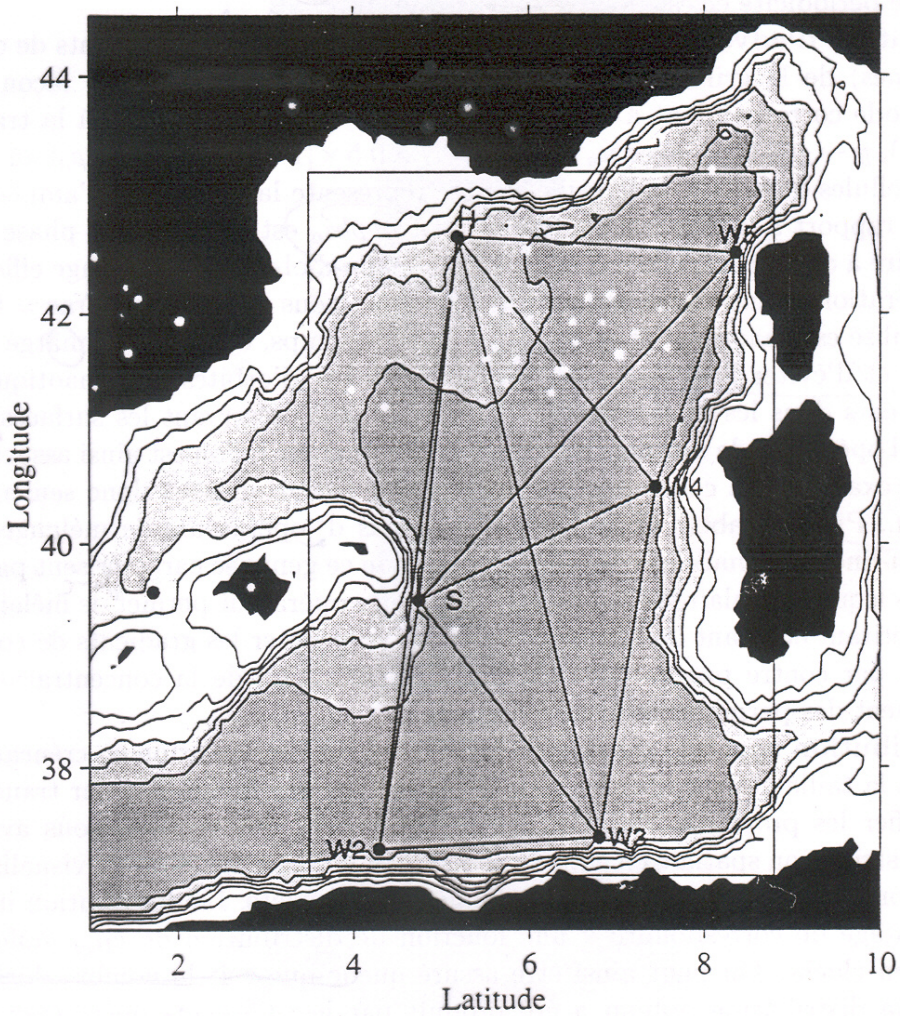

FIG. 1 – *Bassin méditerranéen occidental: réseau d'observation tomographique de l'expérience Thétis 2 et limites du domaine spatial utilisé pour les expériences numériques d'assimilation.*

E. Rémy, Doctoral Dissertation, 1999

Purpose of assimilation : reconstruct as accurately as possible the state of the atmospheric or oceanic flow, using all available appropriate information. The latter essentially consists of

- The observations proper, which vary in nature, resolution and accuracy, and are distributed more or less regularly in space and time.

- The physical laws governing the evolution of the flow, available in practice in the form of a discretized, and necessarily approximate, numerical model.

- 'Asymptotic' properties of the flow, such as, *e*. *g*., geostrophic balance of middle latitudes. Although they basically are necessary consequences of the physical laws which govern the flow, these properties can usefully be explicitly introduced in the assimilation process.

Assimilation is one of many '*inverse problems*' encountered in many fields of science and technology

- solid Earth geophysics
- plasma physics
- 'nondestructive' probing
- navigation (spacecraft, aircraft, ….)
- …

Solution most often (if not always) based on Bayesian, or probabilistic, estimation. 'Equations' are fundamentally the same.

Difficulties specific to assimilation of meteorological observations :

- Very large numerical dimensions ($n \approx 10^6$-10^9 parameters to be estimated, $p \approx 4$-5.10^7 observations per 24-hour period). Difficulty aggravated in Numerical Weather Prediction by the need for the forecast to be ready in time.

- Non-trivial, actually chaotic, underlying dynamics

Cours à venir

~~Vendredi 26 mars~~
~~Vendredi 2 avril~~
Vendredi 9 avril
Vendredi 16 avril
Vendredi 7 mai
Vendredi 14 mai
Vendredi 21 mai
Vendredi 28 mai